NASA CR-121091
SRD-72-163

ABSOLUTE INTENSITY AND POLARIZATION OF ROTATIONAL RAMAN SCATTERING FROM N_2, O_2, AND CO_2

by

C.M. Penney, R.L. St. Peters, and M. Lapp

General Electric Corporate Research and Development

Prepared for

NATIONAL AERONAUTICS AND SPACE ADMINISTRATION

NASA Lewis Research Center

Contract NAS3-15825

1. Report No.	2. Government Accession No.	3. Recipient's Catalog No.
NASA CR 121091		

4. Title and Subtitle	5. Report Date
Absolute Intensity and Polarization of Rotational Raman Scattering from N_2, O_2, and CO_2	January 1973
	6. Performing Organization Code

7. Author(s)	8. Performing Organization Report No.
C. M. Penney, R. L. St. Peters, and M. Lapp	SRD-72-163
	10. Work Unit No.

9. Performing Organization Name and Address	11. Contract or Grant No.
General Electric Company Schenectady, New York 12301	NAS 3-15825
	13. Type of Report and Period Covered

12. Sponsoring Agency Name and Address	13. Type of Report and Period Covered
National Aeronautics and Space Administration Washington, D.C. 20546	Contract Report
	14. Sponsoring Agency Code

15. Supplementary Notes Project Manager - Jack A. Salzman
Chemical Propulsion Division
NASA Lewis Research Center
Cleveland, Ohio

16. Abstract This report presents an experimental examination of the absolute intensity, polarization, and relative line intensities of rotational Raman scattering (RRS) from N_2, O_2, and CO_2. The RRS is excited by laser radiation at two wavelengths: 488.0 and 647.1 nm. The absolute scattering intensity for N_2 is characterized by its differential cross section (summed over Stokes and anti-Stokes bands and over scattered light polarizations) for backscattering of incident light at 647.1 nm, which is calculated from basic measured values to be 4.71×10^{-30} cm^2/sr $\pm 8\%$. The ratio of the corresponding cross section for O_2 to that for N_2 is $2.50 \pm 5\%$. The intensity results for N_2, O_2, and CO_2 are shown to compare favorably to values calculated from recent measurements of the depolarization of Rayleigh scattering plus RRS. Measured depolarizations of various RRS lines agree to within a few percent with the theoretical value of 3/4. Detailed error analyses are presented for intensity and depolarization measurments. Finally, extensive RRS spectra at nominal gas temperatures of 23°, 75°, and 125°C are presented and shown to compare favorably to theoretical predictions.

17. Key Words (Suggested by Author(s))	18. Distribution Statement
Light Scattering Rotational Raman Scattering Absolute Scattering Intensity	Unclassified-Unlimited

19. Security Classif. (of this report)	20. Security Classif. (of this page)	21. No. of Pages	22. Price*
Unclassified	Unclassified	83	

*For sale by the National Technical Information Service, Springfield, Virginia 22151

TABLE OF CONTENTS

SUMMARY

This report presents a detailed, predominantly experimental examination of rotational Raman scattering (RRS) from N_2, O_2 and CO_2, excited by laser radiation at wavelengths of 488.0 nm and 647.1 nm. The purpose of this work is to determine the absolute intensity of RRS and to compare its depolarization and relative line intensities to theoretical predictions.

The pertinent characteristics of RRS are summarized, followed by a detailed description of the experimental apparatus and procedures. Ninety-degree scattering is observed from polarized incident beams. Absolute scattering intensities of RRS spectral lines of N_2 are determined in two ways: by comparison of absolute measurements of incident and scattered light power, and by comparison of RRS and Rayleigh scattering intensities. Scattering intensities for RRS from O_2 and CO_2 are measured relative to that from N_2.

A relationship between the absolute intensity of RRS and the depolarization ρ_T of Rayleigh scattering plus RRS is developed. This relationship is used to show that our intensity results compare favorably to values calculated from recent measurements of ρ_T. Also, expressions for the angle and frequency dependence of RRS are presented. The intensity results for N_2 are characterized by its differential RRS cross section (summed over Stokes and anti-Stokes bands, and over scattered light polarizations) for backscattering of incident light at 647.1 nm, which is calculated from basic measured values to be 4.71×10^{-30} cm^2/sr ±8%. The ratio of the corresponding cross section for O_2 to that for N_2 is 2.50 ±5%.

The depolarizations of strong lines of RRS from N_2, O_2 and CO_2 are determined from changes in the scattering signal when the incident beam polarization is rotated through 90°. The results agree to within a few percent with the theoretical value of 3/4. Detailed error analyses are presented for the intensity and depolarization measurements.

Finally, extensive RRS spectra at nominal gas temperatures of 23°, 75° and 125°C are presented and the relative intensities of the RRS spectral lines are compared to theoretical predictions. Although the deviations of signal levels for individual lines from theoretical predictions are somewhat larger than expected from counting statistics, no systematic departure from theory is evident.

INTRODUCTION

Remote measurements of temperature in gases using rotational Raman scattering (RRS) recently have been proposed (ref. 1) and demonstrated (ref. 2). In addition to this promising application, the properties of spontaneous RRS determine the threshold for stimulated RRS (ref. 3), which may be one of the significant mechanisms affecting the transmission of very high power light beams through the atmosphere (ref. 4). Within these areas of study, it is desirable to know relative and absolute intensities of the spontaneous RRS from different gas molecules. In particular, for experiments in the atmosphere, characteristic RRS intensities for N_2, O_2 and CO_2 are useful.

We have been able to find only one previous direct measurement of RRS intensity for any of these gases. This measurement (ref. 5), for O_2 with 488.0 nm incident radiation, is not accompanied by a full description of the experimental technique nor is an error estimate presented. The intensity of RRS can be calculated indirectly from measurements of the depolarizations of Rayleigh scattering. However, depolarization measurements are difficult because they require determination of a small quantity (the weaker polarization component) in the presence of strong background. Perhaps for this reason, depolarizations measured by different observers have been in poor agreement (ref. 6). Finally, accurate theoretical calculations of RRS intensities, while tractable for H_2 and D_2 (ref. 7), have not been obtained for the heavier gases.

The present interest in RRS intensities, and the paucity of information about these quantities establish a need for additional direct measurements. In this report we present a set of such measurements for N_2, O_2 and CO_2. One purpose of our program was to determine accurate RRS intensities and to present detailed estimates of the expected error of these measurements. A second purpose was to compare the spectral characteristics of the RRS with theoretical predictions at three temperatures (23°C, 75°C, and 150°C). This combination of results should allow the RRS signal to be calculated with reasonable assurance under a variety of experimental conditions.

SCATTERING INTENSITY IN TERMS OF CROSS SECTIONS

Cross sections provide a useful measure of the intensity of light scattering from gases. A cross section σ can be interpreted as the "target area" presented to incident irradiance by a molecule for any particular reaction, such that the flux geometrically incident upon this area will undergo the given

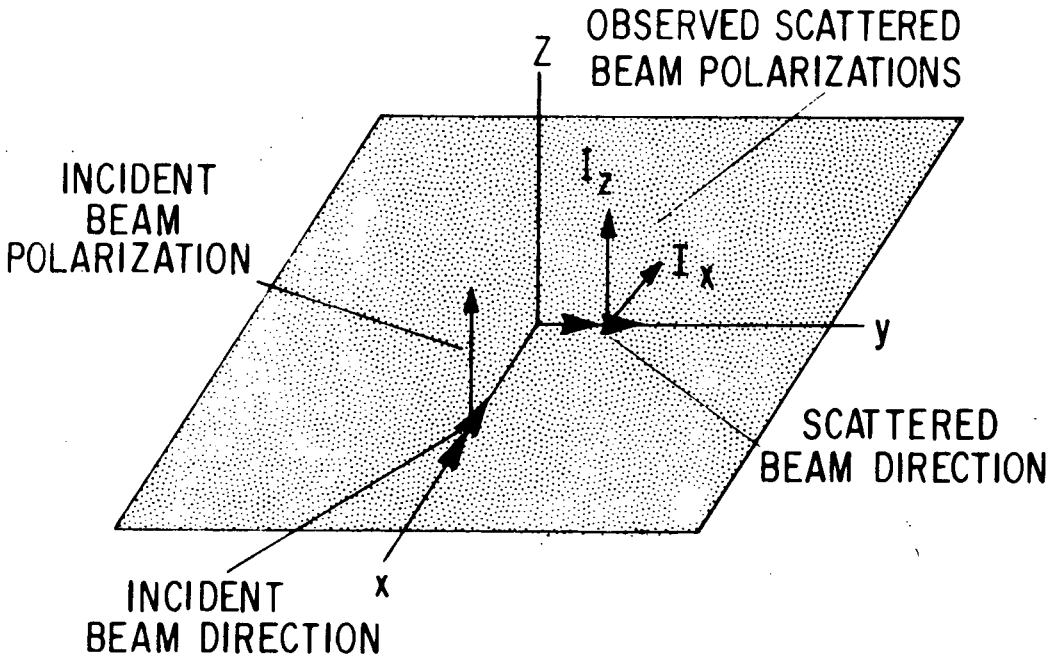

Figure 1. Standard scattering geometry for definition of the cross section σ_{zz} and depolarization ρ.

reaction. It follows that the intensity of light scattered from a segment of an incident beam by a gas is given by

$$I_s(\text{watts/sr}) = P_o(\text{watts})N\left(\frac{\text{molecules}}{\text{cm}^3}\right)F\sigma\left(\frac{\text{cm}^2}{\text{sr}}\right)L(\text{cm}) \quad (1)$$

Here P_o is the incident beam power, N is the number density of molecules, F is the fraction of those molecules which can contribute to the particular type of scattering under observation, and L is the length of the observed scattering volume, measured along the direction of propagation of the incident beam. Because we will be concerned with the angular distribution of scattering, the cross section in Eq. (1) has units of area per unit solid angle (steradian). This quantity is often called a "differential cross section" and denoted by $d\sigma/d\Omega$. However, in this report we will use the simpler designation in order to simplify notation.

The cross section in Eq.(1) contains the angle dependence of the scattering. Under conditions of present interest this scattering can be characterized as dipole scattering from randomly oriented molecules. In this situation the angle dependence of the cross section can be described by a relatively simple form which can be completely specified by two experimental parameters, for example, σ_{zz} and ρ as defined below. Thus, (ref. 8)

$$\sigma = \sigma_{zz}\left((1-\rho)\cos^2\Psi+\rho\right) \quad (2)$$

Here Ψ is the angle between the polarizations of incident and observed scattered light. The quantities σ_{zz} and ρ can be defined in terms of an experimental arrangement involving a linearly polarized incident beam. The cross section σ_{zz} is that relating incident and observed scattered light with polarizations in the same direction. A standard scattering geometry within which this cross section can be measured is shown in Fig. 1. With reference to this figure and Eq.(1),

$$\sigma_{zz} = \frac{I_z}{P_o NFL} \quad (3)$$

where I_z is the intensity of light scattered in the y-direction with polarization in the z-direction.

The depolarization ρ describes the degree of polarization of light scattered in a particular direction, conventionally chosen as the y-direction in the standard scattering geometry of Fig. 1. Thus

$$\rho = \frac{I_x}{I_z} \tag{4}$$

where I_x is the intensity of light scattered in the y-direction with polarization in the x-direction. It is important to emphasize that this definition involves linearly polarized incident light. An alternative depolarization factor, which we shall designate by ρ', is used in much of the older literature. This depolarization is defined as the intensity ratio I_x/I_z obtained with unpolarized incident light. The relationship between the two depolarization factors is

$$\rho' = \frac{2\rho}{1-\rho} \tag{5}$$

Using Eq. 2, the scattering cross section for many special cases of interest can be expressed directly in terms of σ_{zz} and ρ. If the incident light is unpolarized it may be divided equally between two convenient orthogonal polarizations and the separate contributions summed. If the observed scattered light is not polarization-analyzed, then a sum over convenient orthogonal polarizations of scattered light is appropriate. For example, the cross section for unanalyzed backscattering is

$$\sigma = \sigma_{zz}\,(1+\rho) \tag{6}$$

for both polarized and unpolarized incident light. On the other hand if the incident light is linearly polarized, and backscattering with the orthogonal polarization is observed, the corresponding cross section is

$$\sigma = \rho\sigma_{zz} \tag{7}$$

Finally, the appropriate cross sections for more complicated geometries can be determined using the coordinate system shown in Fig. 11 of Appendix A. In particular, the total cross section, integrated over all angles and summed over scattered light polarization, is given by

$$\sigma^T = \frac{8\pi}{3}\,\sigma_{zz}(1+2\rho)\,. \tag{8}$$

CHARACTERISTICS OF ROTATIONAL RAMAN SCATTERING CROSS SECTIONS

A spectrum of pure RRS consists of a series of lines spread on either side of the exciting line, often assuming an "angel

wing" configuration about the exciting line. Characteristics of such spectra are discussed in detail in several references. (See for example, ref. 9, pp. 61-141 and ref. 10, pp. 40-94.) In the following paragraphs we present a brief summary of those characteristics relevant to the present work. This discussion will be confined to the special case of a simple linear molecule (SLM); i.e., a linear molecule in states with no electronic angular momentum. This special case applies directly to N_2 at temperatures below that at which appreciable electronic excitation occurs. It is not completely correct for either O_2 or CO_2, because of the ground state electron spin in O_2 (ref. 11), and the non-symmetric vibrational state of CO_2 which is significantly populated ($\sim$8%) at room temperature (ref. 12). However, the deviation between the RRS spectra for these molecules and that for a SLM appears to be sufficiently small to be neglected in atmospheric temperature measurements. These deviations are discussed more fully in Appendix B.

Placzek showed (ref. 9, pp. 40) that the scattering from randomly oriented molecules can be broken up into three components, which he called trace scattering, quadrupole scattering and magnetic dipole scattering. (All of these components arise through the dipole approximation; the latter two are so-named because their selection rules are the same as those for true quadrupole and magnetic dipole scattering.) Non-resonance RRS from SLM is composed solely of quadrupole scattering. The corresponding selection rules allow the following transitions:

$$J \rightarrow J + 2$$

$$J \rightarrow J - 2 \quad (\text{for } J \geq 2)$$

$$J \rightarrow J \quad (\text{for } J \neq 0).$$

Transitions of the first type lead to a rotational state with greater energy than the initial state; consequently, the scattered light is shifted to the red of the incident light (Stokes RRS). Likewise, the second transition leads to scattered light shifted to the blue (anti-Stokes RRS). Finally, the third transition (Q-Branch) leads to unshifted scattering and thus contributes to the Rayleigh scattering.

The spectral shift of each line from the exciting line, $\omega_{J \rightarrow J'}$, can be expressed in terms of the rotational constant B_o and the rotational quantum number of the initial state. Thus in terms of wave numbers

$$\omega_{J \rightarrow J+2} = - (4J+6) B_o \tag{9}$$

$$\omega_{J \rightarrow J-2} = (4J-2) B_o \tag{10}$$

and of course

$$\omega_{J\to J} = 0 \tag{11}$$

Here and subsequently we omit higher order terms in J because the corrections they contribute are negligible under conditions of present interest.

The dependence of any particular RRS line intensity on the characteristics of the gas can be expressed conveniently in the following form.

$$I_{J\to J'} = ANF_J\sigma_{J\to J'} \tag{12}$$

The constant A contains the optical parameters of the system, N is the number density of molecules, F_J is the population fraction of molecules in the initial states which contribute to the observed line and $\sigma_{J\to J'}$ is the cross section for quadrupole scattering.

For a gas in thermodynamic equilibrium, the population fraction can be expressed in the form

$$F_J = g_J\ (2J+1)\ \exp\ (-E_J/k\Theta)/Q \tag{13}$$

Here g_J is a statistical weight factor determined by symmetry considerations involving nuclear spin, E_J is the rotational energy of the molecule in the Jth rotational state, Θ is the absolute temperature, k is the Boltzmann constant, and Q is the rotational partition function, chosen such that

$$\sum_{J=0}^{\infty} F_J = 1 \tag{14}$$

The factor g_J assumes the values shown in Table 1.

Table 1: Values of the statistical weight factor.

	Even Rotational Quantum Number	Odd Rotational Quantum Number
O_2	0	1
N_2	6	3
CO_2	0	1

The rotational energy is given by

$$E_J = hcB_o J(J+1) \tag{15}$$

The cross section $(\sigma_{zz})_{J\to J'}$ can be broken up further as follows:

$$(\sigma_{zz})_{J\to J'} = b_{J\to J'} \left[\frac{\omega_o + \omega_{J\to J'}}{\omega_o}\right]^4 U\,\omega_o^4 \tag{16}$$

Here $b_{J\to J'}$ is a Placzek-Teller coefficient (a known function of incident final rotational quantum numbers), ω_o is the wave number of the incident light, the factor $[\omega_o + \omega_{J\to J'}]^4$ thus expresses the well known fourth power dependence of the cross section of the scattering wavenumber, and U is a factor which is nearly independent of frequency and J-value for each molecule. The Placzek-Teller coefficients for a SLM are:

$$b_{J\to J+2} = \frac{3(J+1)(J+2)}{2(2J+1)(2J+3)} \tag{17}$$

$$b_{J\to J-2} = \frac{3J(J-1)}{2(2J+1)(2J-1)} \tag{18}$$

$$b_{J\to J} = \frac{J(J+1)}{(2J-1)(2J+3)} \tag{19}$$

Expression of the cross section in the form of Eq. (16) is convenient because the first two factors are known functions of J and/or ω_o, and from theoretical considerations the third factor U is expected to be nearly constant away from resonance. This expectation is supported by experimental and theoretical results to be described subsequently in this report. Thus a measurement of the intensity of any RRS line will allow determination of U, and from this "constant", the intensity of other lines can be calculated. From the preceeding equations one obtains for a Stokes line

$$(I_z)_{J\to J+2} = ANF_J \frac{3(J+1)(J+2)}{2(2J+1)(2J+3)} \left[\frac{\omega_o - (4J+6)B_o}{\omega_o}\right]^4 U\omega_o^4 \tag{20}$$

Similarly, for an anti-Stokes line

$$(I_z)_{J\to J-2} = ANF_J \frac{3J(J-1)}{2(2J+1)(2J-1)} \left[\frac{\omega_o + (4J-2)B_o}{\omega_o}\right]^{-4} U\omega_o^4 \tag{21}$$

and for the Q-branch (contribution to Rayleigh scattering)

$$(I_z)_{J\to J} = ANF_J \frac{J(J+1)}{(2J-1)(2J+3)} U\omega_o^4 \tag{22}$$

One of the important characteristics of quadrupole scattering is that its theoretical depolarization, and hence that of RRS, is

$$\rho_q = 3/4 \tag{23}$$

This result is on a firm basis for isolated molecules. Collisions in a gas are likely to change the depolarization, but we expect that the magnitude of this effect at pressures near STP is very small.

Theoretical expressions for the depolarized components $(I_x)_{J\to J'}$ can be obtained from Eqs. (20), (21) and (22) through multiplication by the theoretical depolarization ρ_q. Also of interest are the sums of the scattering components over all J-values. These sums can be expressed in terms of

$$S_S \equiv \sum_{J=0}^{\infty} F_J \, b_{J\to J-2} \left[\frac{\omega_o - (4J+6)B_o}{\omega_o}\right]^4 \tag{24}$$

$$S_{AS} \equiv \sum_{J=0}^{\infty} F_J \, b_{J\to J+2} \left[\frac{\omega_o + (4J-2)B_o}{\omega_o}\right]^4 \tag{25}$$

$$S_Q \equiv \sum_{J=0}^{\infty} F_J \, b_{J\to J} \tag{26}$$

and

$$S = S_S + S_{AS} + S_Q \tag{27}$$

These quantities are nearly independent of incident wavelength and temperature over the range of present interest (400.0-700.0 nm and >100°K). Representative values for N_2 and O_2 are shown in Table 2. These values may be used, for example, to calculate the sum of the cross section $(\sigma_{zz})_{J\to J'}$ over all RRS lines. Thus

$$(\sigma_{zz})_{RRS} = U\omega_o^4 \, [S_S + S_{AS}] \tag{28}$$

An important relationship between depolarization of Rayleigh scattering and RRS scattering intensities can be established through the following considerations:

Table 2. Values of the sums S_S, S_{AS}, S_Q, and S, for N_2, O_2, and CO_2 treated as simple linear molecules. The rotationl constants B_o for N_2 and O_2 are obtained from Ref. 10 and for CO_2, from Gerhard Herzberg, Molecular Spectra and Molecular Structure II. Infrared and Raman Spectra D. VanNostrand, Princeton, N.J., 1945.

Molecule	B_o in cm^{-1}	λ_o in nm	Θ in°K	S_S	S_{AS}	S_Q	S
N_2	2.0007	488.0	223	.4410	.3004	.2563	.9977
			296	.4311	.3114	.2553	.9977
			323	.4282	.3145	.2550	.9977
		647.1	296	.4290	.3128	.2553	.9970
		694.3	296	.4284	.3132	.2553	.9968
O_2	1.4298	488.0	296	.4200	.3187	.2596	.9984
		647.1	296	.4183	.3199	.2596	.9979
		694.3	296	.4178	.3203	.2596	.9977
CO_2	.3895	488.0	296	.3998	.3467	.2531	.9996
		647.1	296	.3990	.3474	.2531	.9994
		694.3	296	.3987	.3476	.2531	.9994

As noted above RRS is pure quadrupole scattering, whereas non-resonance Rayleigh scattering from SLM is composed solely of quadrupole scattering and trace scattering. Trace scattering is completely polarized ($\rho_t=0$) and its magnitude can be expressed in terms of the refractive index n of the gas at any particular molecule number density N. This relationship can be put into the form

$$\sigma^t = 4\pi^2 \omega_o^4 \left(\frac{n-1}{N}\right)^2 \tag{29}$$

The total contributions to the polarized Rayleigh scattering intensity I_z is

$$I_z = AN(\sigma^t + U\omega_o^4 SQ) \tag{30}$$

whereas the total contribution to the depolarized Rayleigh scattering intensity I_x comes from the quadrupole scattering; i.e.

$$I_x = (3/4)ANU\omega_o^4 S_Q \tag{31}$$

Here the factor 3/4 represents the depolarization of quadrupole scattering (Eq. 23). Thus the depolarization of Rayleigh scattering is given by

$$\rho_{RAY} = 3/4 \frac{U\omega_o^4 S_Q}{\sigma^t + U\omega_o^4 S_Q} \tag{32}$$

Likewise, the depolarization of the band comprising Rayleigh scattering plus both branches of the RRS is

$$\rho_T = 3/4 \frac{U\omega_o^4 S}{\sigma^t + U\omega_o^4 S} \tag{33}$$

It is useful to note that S is very nearly equal to unity in cases of present interest. Since σ^t can be calculated from Eq. (29), these expressions allow calculations of U from measurements of ρ_{RAY} or ρ_T. Recent measurements of ρ will be used subsequently in this report to obtain comparisons with our experimental results.

MEASUREMENT OF RRS CROSS SECTIONS

Alternative Methods for Absolute Cross Section Measurements

In principle, determination of a light scattering cross section involves a relative measurement of incident and scattered light power. In the case of Raman scattering cross sections, this measurement is made difficult by two factors:

first, the incident and scattered light are at different wavelengths; second, the scattered light power to be measured is typically 10^{-15} of the incident light power. The first factor necessitates a relative spectral calibration of the optical device used to isolate and detect the scattered light. The second factor has inspired substantial ingenuity in attempts to relate the measurement of incident and scattered light. It is worthwhile to mention some of the techniques which have been developed for this purpose in order to explain the procedure we have adopted.

Use of Attenuating Filters: One approach is to measure the incident and scattered light with the same detector. Then only a relative spectral calibration for the detector is needed to determine a Raman cross section. Unfortunately, no practical light detector has a linear range over the required 10^{15} variation of light power. However, attenuating filters can be used to allow measurement of the incident and scattered light with the same detector. Calibrated attentuations as large as 10^{12} to 10^{14} are obtained by using several filters in series. The attenuation of each filter is measured separately. The total attenuation is then assumed to be equal to the product of individual attenuations. In using this approach great care must be taken to account for the spatial variation of detector sensitivity and filter transmission. Furthermore, the possibility of filter saturation and changes in filter transmission with time in the intense laser beam must be examined.

Comparison to Rayleigh Scattering: Absolute Raman scattering cross sections can be measured by comparison to a presumable known cross section, such as a Rayleigh cross section. The Rayleigh cross section and refractive index for a molecule in a gas are related by (ref. 8, p. 40).

$$(\sigma_{zz})_{RAY} = \frac{4\pi^2}{\lambda_o^4} \left(\frac{n-1}{N}\right)^2 \left(\frac{3}{3-4\rho_{RAY}}\right) \tag{34}$$

Here n is the refractive index of the molecules at a density of N molecules/unit volume, and ρ_{RAY} is the depolarization of the Rayleigh scattering. Eq.(34) is in good agreement with recent experimental results (ref. 6). Rayleigh scattering cross sections are typically 10^3 to 10^4 times larger than the corresponding vibrational Raman scattering cross sections. Thus it is possible to compare the cross sections within a large but not impractical linear detection range, checked by changes in incident light power and gas pressure. Furthermore, the spatial distribution of the Rayleigh and Raman scattering are identical, which relaxes problems introduced by spatial variations in the response of the detection system. The major problem with this approach is that Mie scattering from small particles in the gas

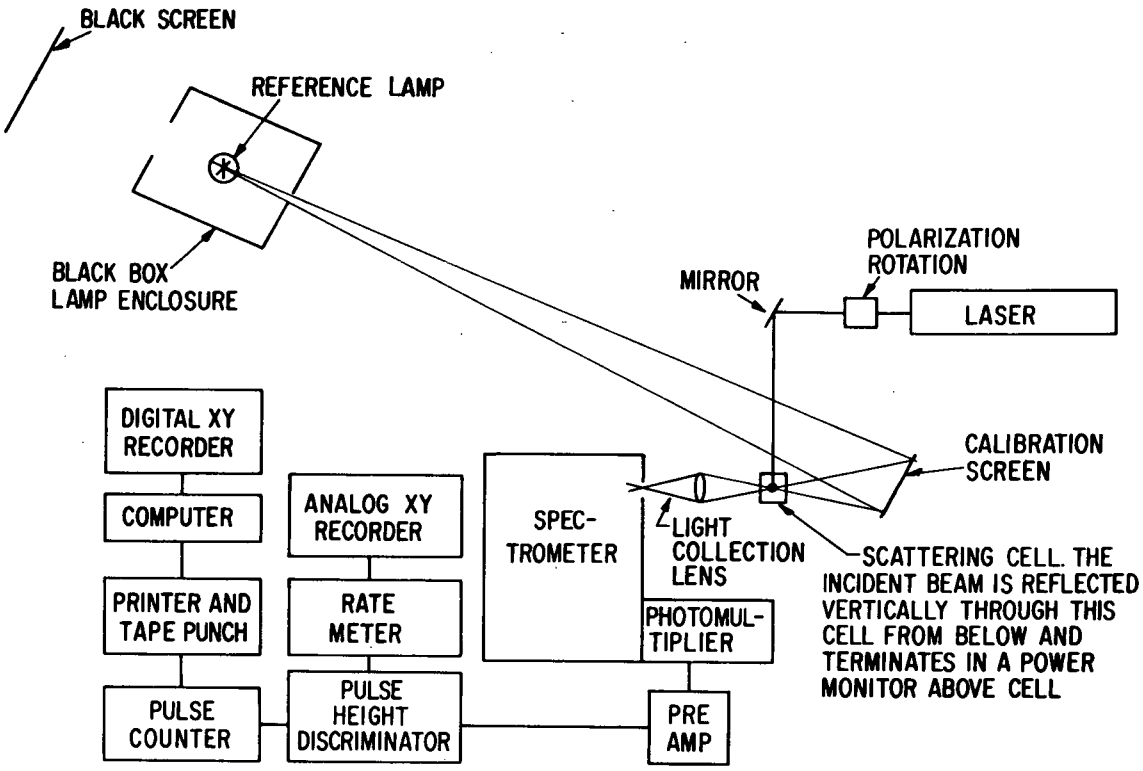

Figure 2. Schematic diagram of the system used to observe rotational Raman scattering.

is inseparable (within a typical spectrometer system) from the Rayleigh scattering. Therefore, if enough particles are present to cause significant Mie scattering in comparison to the Rayleigh scattering, the Rayleigh cross section calculated from the experimental data (assuming no particles) will be larger than the true cross section, and measured Raman-to-Rayleigh ratios will err on the small side. In practice, careful filling procedures, ultramicroscope techniques, comparison of scattering with different gas pressures and compositions, and gravitational and electrostatic sedimentation can be used to ensure negligible particle contributions.

Comparison to Rotational Raman Scattering from H_2: Another cross section which can be calculated from theory is that for the pure rotational Raman scattering from H_2. Schrötter and Bernstein (ref.13) used this cross section for the J=1 → 3 line in H_2 to obtain absolute vibrational Raman cross sections by comparison. This approach is advantageous in that the rotational line is separated from the Mie scattering (and scattering from various walls, windows, etc.) by a spectral shift of 587 cm^{-1}. Furthermore it is closer than Rayleigh scattering to the Raman scattering, both spectrally and in intensity. However, calculation of the magnitude of this cross section is not on as firm a theoretical basis as calculation of the Rayleigh cross section from measured values of the refractive index.

Combination of Two Absolute Measurements: In this approach separate absolute calibrations for the detectors of incident and scattered radiation are used. One advantage of this approach is that it does not depend on reference theoretical cross sections or the vagaries of attenuation filters. However, the accuracy of absolute calibrations is generally poorer than that of relative calibrations. Furthermore, as with the filter method, care must be taken to account for spatial variations in detector sensitivity.

Methods Used in Present Work: Our cross section measurements were obtained by combination of two absolute measurements, and simultaneously by comparison to Rayleigh scattering. Both results for each gas are accessible from the data presented in a later section. The experimental configuration used in these measurements is illustrated in Fig. 2. The components of the experimental system are described in the next section, followed by a detailed description of the methods used in the cross section measurements.

Description of Experimental System

The light sources used in this work are CRL Model 52B argon and Krypton ion lasers. The argon laser provides up to 1.5 watts of light at 488.0 nm, and the krypton laser, 0.6 watts at 647.1 nm. Both lasers are regulated internally to a power stability better than ±1%. This power regulation is verified

by the external thermopile monitor above the scattering cell. The polarization of the output beam is linear to better than one part in 10^2. It was rotated to desired orientations by a Spectra Physics Model 310-21 polarization rotator.

The incident beam was focussed from a $1/e^2$ diameter of about 3 mm by a 25 cm focal length quartz lens, producing a beam with a diameter of about 100μm in the scattering region. The laser power was measured by a CRL thermopile with a spectral response certified flat and accurate to within 10% over the wavelength range encountered in these experiments. The observed gases were contained within a simple cylindrical cell. Measurements at elevated temperatures were accomplished by enclosing the cell within an oven. The cell temperature was monitored by a chromel-alumel thermocouple and a glass thermometer, both in contact with the cell.

The gases used in this work were obtained from new lecture bottles with the following designations: Nitrogen-Matheson Prepurified Grade; Methane-Matheson Ultra High Purity; Oxygen-Union Carbide (Linde) Extra Dry Grade; Carbon Dioxide-Union Carbide Bone Dry Grade. Published assays of these grades indicate no impurity levels which should affect our measurements.

The gas handling system is constructed of stainless steel and pyrex with Teflon gaskets. The system will maintain a pressure of 2μm Hg (no observable pressure increase in several hours) after pump-down by a two-stage mechanical pump and liquid nitrogen cold trap. Pressures were monitored by a thermocouple guage and precision pressure measurements were obtained using a Hg manometer with dry ice cold trap.

The scattered light was analyzed by a Spex Model 1400-11 3/4 meter double Czerny Turner monochromator using 1200 lines/mm Bausch and Lomb gratings blazed at 5000Å. The linear reciprocal dispersion of this instrument is shown in Table 3.

Table 3. Reciprocal dispersion of the Spex 1400-11 spectrometer in first order, with 1200 groove/mm gratings

Wavelength (nm)	Reciprocal dispersion (nm/mm)
197.0	.555
428.2	.550
632.8	.535
827.3	.510
1060.0	.465

The detector is a cooled (-50°C) RCA C31000E extended red response photomultiplier. The photomultiplier signal was processed by a pulse counting system composed of a preamplifier, Hamner amplifier and pulse height discriminator, an electronic

counter, a printer and tape punch, and an analog pulse rate meter used to drive xy-recorders. In most cases a Wollensak 75 mm focal length f/1.9 camera lens was used to collect scattered light and to focus it within the monochromator entrance slit under a magnification of 0.8X.

The absolute spectral calibration of the collection lens-monochromator-photomultiplier system was accomplished in the following manner: A GE 200W halogen quartz reference lamp (ref. 14) enclosed in a large (75 cm cube) black box with a small aperture was used to illuminate a nearly perfect Lambertian scattering screen from a distance of several meters. The reference lamp was calibrated by Eppley Laboratory, Inc. from 300 nm to 1.1μm and checked by comparison against a second lamp calibrated by Optronic Laboratories, Inc. The comparison was consistent with the calibrations to within 10% absolute over the spectral range involved in the present measurements. The scattering screen was constructed by flowing barium sulphate in a liquid suspension supplied by Eastman Kodak (ref. 15) onto a 1/2" thick aluminum plate. The area to be covered was milled out to a depth of 1/16" and sandblasted. The barium sulphate coating was built up in several steps, with intervening slow (∿1 day) drying in an enclosed space, and finally scraped with a sharp-edged glass plate back to a thickness of 1/16". Through a direct comparison of incident and scattered light, this screen was found to approximate a perfect Lambertian scatterer to within experimental error of 3% at a scattering angle of 30°, with incident light normal to the screen, over the spectral range from 450 nm to 500 nm, and separately, over the range from 500 nm to 650 nm. These spectral ranges were isolated using filters.

The light from the reference lamp was diffusely scattered by the screen and then passed through the gas cell. Part of this light was collected by the collection lens and focused through the monochromator entrance slit. A polarization filter near the slit was used to determine the response of the monochromator to light polarized parallel and perpendicular to the grooves of the spectrometer gratings. Transmission of the monochromator for second order was shown to be negligible by a filter technique.

The optical arrangement provides the following important advantages:

1. The reference count rate and Raman count rate can be made approximately equal with convenient slit settings and reference lamp-to-screen distance. In our work the reference lamp was placed at a distance of 3 to 4 meters from the scattering screen, and the slit settings used in reference measurements were typically 300μm x .5 cm (entrance), 3000μm (intermediate), and 300μm (exit). These slit widths are sufficiently large to avoid significant diffraction and polarization effects.

2. All of the light from the reference lamps collected by the lens and subsequently focused through the entrance slit of the spectrometer must pass through the virtual image of the entrance slit within the scattering cell. Since the scattered light emanates from the same region, spatial variations in system response should not introduce significant calibration errors.

3. The calibration of the system can be checked using the reference lamp during each measurement, even with the cell in place.

Analysis of System

A straightforward ray-tracing analysis yields expressions for the photomultiplier count rate under exposure to the reference and scattered light. The reference light measurements provide the relative response of the spectrometer system to light of various polarizations, a relative spectral calibration of this system used in the comparison of RRS to Rayleigh scattering, and an absolute calibration used in the determination of cross sections from absolute measurements of scattering and incident light.

To determine the response of the system to the reference lamp, we assume (for the moment) that the barium sulphate screen is a perfect Lambertian scatterer. Then the radiant flux (watts/cm^2 sr nm) in a direction normal to any surface above the screen is equal to the normal brightness B_λ of the screen (in the same units). This brightness is given by

$$B_\lambda = I_\lambda/\pi \tag{35}$$

where I_λ is the irradiance provided by the calibrated lamp at the screen.

When all of the optical elements of the spectrometer system (including the scattering cell) are in proper alignment for a scattering experiment, then the virtual image of the entrance slit formed by the collection lens must coincide with the scattering volume (that segment of the incident beam from which scattering is observed). Furthermore, all of the light from the reference screen which passes through the spectrometer must also pass through this volume. Consequently the reference and scattered light have nearly the same spatial distribution at the slit virtual image and traverse the same paths from the scattering volume to the detector.

The response to the reference light under these conditions, with no polarization filter in place, is

$$C_o\left(\frac{\text{counts}}{\text{sec}}\right) = T_1 T_2 \left\langle \frac{1}{\cos\mu} \right\rangle \frac{I_\lambda \Omega w \ell w_e \Delta}{2\pi} [R_\perp + R_\parallel] \qquad (36)$$

Here T_1 is the transmission of the front (closest to spectrometer) window of the cell and T_2 is the transmission of the opposite window. Transmission factor T_1 includes a small correction for multiple reflections in the cell. The angle μ is that between the spectrometer axis and the direction along which any particular ray of reference light passes through the cell. The angle brackets indicate an average of $1/\cos\mu$ over all angles accepted by the spectrometer. This average is insignificantly different from 1 in the present case, and thus will be omitted subsequently.

The solid angle accepted by the spectrometer is Ω, and w and ℓ are entrance slit width and length, respectively. The exit slit width is w_e and the reciprocal dispersion of the spectrometer is Δ.

The quantity $R_\perp$ is defined to be the system response (in counts per second per watt) to light with polarization perpendicular to the grating grooves which passes through the virtual image of the slit, is focused by the collection lens within the solid angle accepted by the spectrometer, and is within the spectral range passed by the exit slit. The quantity $R_\parallel$ is similarly defined for light polarized parallel to the grating grooves. We note that I_λ, Δ, Ω, $R_\perp$ and $R_\parallel$ all can be expected to vary significantly with wavelength.

When a linear polarizer with transmission T_p (to linearly polarized light with optimum orientation) and effectively infinite extinction ratio is placed in front of the slit and oriented to pass light with polarization perpendicular to the grating grooves, the resulting count rate is

$$C_\perp = T_1 T_2 \frac{I_\lambda \Omega w \ell w_e \Delta}{2\pi} T_p R_\perp \qquad (37)$$

If the polarizer is rotated to pass light parallel to the grating grooves, then the count rate is

$$C_\parallel = T_1 T_2 \frac{I_\lambda \Omega w \ell w_e \Delta}{2\pi} T_p R_\parallel \qquad (38)$$

It is convenient to introduce the parameter

$$\alpha \equiv R_\parallel / R_\perp = C_\parallel / C_\perp \qquad (39)$$

where the equality follows from Eqs(37) and (38). We note that α can be measured by a simple experiment, which involves rotating a polarizer in front of the entrance slit. In practice it is found that α varies significantly with wavelength because of the polarization dependence of grating reflectivity. Thus it is necessary to measure it at frequent wavelength points, or at each wavelength point of interest.

From Eqs.(36) and (39) we obtain

$$C_o = T_1 T_2 \frac{I_\lambda \Omega w \ell w_e \Delta}{2\pi} R_\perp (1+\alpha) \tag{40}$$

Now we will consider the response to Rayleigh or Raman scattering. In our cross section measurements the entrance and exit slits of the monochromator are usually set so that the entrance slit is wider than the focused image of the Raman scattering at that slit, and so that the exit slit is sufficiently wide to pass all of the light of the scattered band of interest. In this situation the response (with no polarization filter) is

$$C_o^s = (T_1 P_o / T_4) N \ell \Omega M F \sigma_{zz} R_\perp (1+\rho\alpha) \tag{41}$$

Here, in addition to quantities defined previously, T_4 is the transmission of the incident beam through the cell wall where it exits the cell, P_o is the incident beam power measured <u>after</u> it passes through the cell, N is the number density of molecules within the cell, M is the magnification of the collection lens, and ρ is the depolarization of the observed scattered light.

With the polarization filter in place and oriented to pass scattered light polarized parallel to the grating grooves, the response is

$$C_\perp^s = (T_1 P_o / T_4) N \ell \Omega M T_p R_\perp F \sigma_{zz} \tag{42}$$

Likewise, with the polarization filter oriented to pass light polarized perpendicular to the grating grooves, the response can be expressed in the form

$$C_\parallel^s = (T_1 P_1 / T_4) N \ell \Omega M T_p R_\perp F \sigma_{zz} \rho\alpha \tag{43}$$

From these equations we obtain

$$\rho = C_\parallel^s / \alpha C_\perp^s \tag{44}$$

Thus the depolarization of a band of scattered light can be determined by measurement of C_x^s and C_z^s along with separate measurement of α using the reference light.

A convenient expression for the cross section in terms of known and measured quantities can be obtained by substituting for $R_\perp$ from Eq.(40) into Eq.(41), and solving for σ_{zz}. This operation yields

$$F\sigma_{zz} = T_2 T_4 \left(\frac{C_o^s}{P_o N}\right) \frac{I_\lambda w w_e \Delta (1+\alpha)}{2\pi C_o M (1+\rho\alpha)} \qquad (45)$$

Eq.(45) allows a calculation of the absolute cross section. The quantities involved in this calculation which have the largest experimental uncertainty are the reference lamp intensity I_λ and the incident beam power P_o. The expected relative errors for these quantities are about 15% and 10%, respectively, based on manufacturer's certifications and our past experience. These uncertainties are the predominant contributions to the estimated error in the cross section determination from absolute measurements.

Substantially smaller estimated errors result when a Raman cross section is measured relative to a Rayleigh cross section, and the absolute Raman cross section is calculated subsequently from the Raman-Rayleigh ratio and the theoretical value for the Rayleigh cross section. In this case only relative power measurements and relative reference lamp irradiance (at the Rayleigh and Raman wavelengths) are involved. The expected errors for each of these relative measurements are less than ±5%.

Experimental Procedure for Nitrogen Cross Section Measurements

The following procedure was used in the measurement of oxygen and nitrogen rotational Raman cross sections:

1. The incident beam is aligned along a vertical axis intersecting the monochromator axis. Then the collector lens is aligned and focused visually on the Rayleigh scattering from an appropriate gas in the cell, using a periscopic microscope to view the scattering from behind the monochromator entrance slit. Final alignment is checked photoelectrically.

2. The entrance slits are set substantially wider than the Rayleigh scattering image of the incident beam. The exit slits are set to provide a flat-topped slit function but allow resolution of single RRS lines. Typical settings at 647.1 nm with the 0.8X magnification system are 200/1000/400/5000μm. In this designation the numbers refer to entrance slit width, intermediate slit width, exit slit width, and entrance slit length, respectively.

3. With the cell evacuated, the incident beam power level is adjusted to a level (usually about 75mW) which yields between 1000 and 2000 counts per second when the monochromator is set on the incident line. These counts come from the incident beam scattering off the cell walls, lens mount, etc.

4. The vacuum system and cell are flushed several times by filling the cell with N_2 to approximately 700 torr and then evacuating the system. Subsequently the count rate is determined at several N_2 pressures (typically 20, 40, and 60 torr). Gas pressures are monitored using the Hg manometer. The Rayleigh scattering image is checked periodically using the microscope behind the entrance slit to verify the absence of visible particles. This measurement is used to calculate the N_2 Rayleigh scattering cross section.

5. This procedure is repeated with several other gases (typically O_2 and methane). The resultant relative count rates are compared to relative theoretical values to obtain further evidence that particle scattering is negligible.

6. With the cell evacuated, and scattered laser light illuminating the reference screen, the monochromator is swept over the incident light and Raman scattering wavelength regions to determine the slit function and background.

7. Reference count rates C_o, $C_\perp$ and $C_\parallel$ are obtained with the reference screen uncovered and the monochromator set at Rayleigh and Raman scattering wavelengths.

8. The reference screen is covered and the vacuum system and cell are flushed several times with N_2. Then the cell is filled slowly with N_2 to about 740 torr and the Raman scattering signal is determined. In a typical measurement the count rate for three of the strongest lines of the Stokes or anti-Stokes RRS is measured in a slow sweep (50 sec/Å) through the appropriate wavelength region.

9. Dark noise background is measured by blocking the laser beam.

Over a period of three months (July through September, 1972) a total of five experiments to measure N_2 RRS cross sections were completed. The optical parameters of the system (magnification of the collection lens, slit settings, spectral region observed, etc.) were varied intentionally in an attempt to uncover any sources of systematic error. Data was analyzed directly from the teletype print-out of the photomultiplier count rate. In many of the N_2 measurements, the slit settings were too wide to allow the signal to return completely to background between RRS lines. In these cases, background was set equal to the measured "dark" count rate with the incident beam

blocked (usually 6 to 7 counts/sec) plus the coutn rate estimated for the small fraction of Rayleigh scattering transmitted through the spectrometer when set at the RRS wavelength ($\sim$ 1.5 counts/sec.) This estimate was obtained from an auxiliary measurement in which the reference screen was illuminated by the appropriate amount of scattered laser light to simulate Rayleigh scattering, and viewed through the evacuated scattering cell by the monochromator system. In each experiment, count rates for several strong RRS lines were obtained and, in a preliminary check, compared against theoretical predictions. From data conforming within expected statistical fluctuations, $F\sigma$ and U for a particular line were calculated, using Eq. (16) and (45). Hand calculations were checked for numerical accuracy by a computer calculation.

Additional Auxiliary Measurements

In order to determine absolute cross sections it is necessary to know the values of w, w_e, T_1 and T_4 in addition to those quantities whose measurement has been discussed previously. The micrometer readings of slit widths w and w_e were checked using a microscope with travelling cross hairs and a precision comparison reticule. The micrometer readings were found to be accurate and repeatable to within measurement error ($\pm 5\mu m$). Subsequently, the magnification M was measured by viewing the image of the comparison reticule through the entrance slits using the periscope. Cell transmission T_1 was calculated by determining the change in reference count rate when the cell was removed, and correcting for multiple reflections, whereas T_4 was calculated from the laser beam transmission through the cell. The estimated values are

$$T_1 = 0.965 \qquad T_4 = 0.95$$

which is consistent with Fresnel reflection losses.

Experimental Procedure for O_2 and CO_2 Cross Section Measurements

Oxygen: Cross sections were determined relative to N_2 cross sections. The spectrometer was swept over several O_2 and N_2 RRS lines within the same spectral region in succession.[2] Each sequence of lines was compared to theoretical intensith calculations to determine if the experimental and theoretical data agreed to within expected statistical fluctuations. From conforming data sets relative O_2 line intensities were determined for individual lines of O_2 and N_2. The ratio of line intensities can be designated by

$$D \equiv \frac{(\text{net count rate})\ O_2,\ N \to N'}{(\text{net count rate})\ N_2,\ J \to J'} \quad \frac{p(N_2)}{p(O_2)} \tag{46}$$

where $p(N_2)$ and $p(O_2)$ represent the respective gas pressures. In Eq. (46) and subsequently we follow the customary practice of using the symbol N to designate the rotational angular momentum of the oxygen molecule. (See Appendix B). A temperature correction does not appear in Eq. (46) because the temperature remained within one degree C range around 23° during these measurements. The ratio D can be expressed in terms of U-values using Eq. (16), which yields

$$D \equiv \frac{F_N b_{N\to N'} (\omega_o + \omega_{N\to N'})^4 U(O_2, \lambda_o)}{F_J b_{J\to J'} (\omega_o + \omega_{J\to J'})^4 U(N_2, \lambda_o)} \tag{47}$$

This equation was used to calculate U-values for O_2 from those for N_2.

Carbon Dioxide: The monochromator was swept over several lines of N_2 and the same spectral region of RRS from CO_2 in quick succession. Although the RRS of N_2 was resolved, several lines of CO_2 were observed simultaneously within the relatively broad slit function, which was not changed between N_2 and CO_2 measurements. A theoretical relative spectrum $C(\lambda)$ for the CO_2 RRS was calculated from the following expression.

$$C(\lambda) \propto \sum_J S(\lambda - \lambda_J) F_J b_{J\to J'} (\omega_o - \omega_{J\to J'})^4 \tag{48}$$

Here $S(\lambda')$ is the slit function, measured ib an auxiliary experiment. The CO_2 and N_2 spectra were checked against theoretical predictions, as in the case of the O_2 measurements. From conforming data sets, U-values for CO_2 were calculated from experimental line intensity ratios $D(\lambda)$, using the following expression:

$$D(\lambda) = \frac{U(CO_2, \lambda_o) C(\lambda)}{U(N_2, \lambda_o) [F_J b_{J\to J'} (\omega_o - \omega_{J\to J'})^4]_{N_2}} \tag{49}$$

RESULTS FOR CROSS SECTION MEASUREMENTS

Nitrogen

The results for the RRS cross section measurements for N_2 are shown in Table 4. The U-values can be used, for example, with Eq. (16) to calculate the cross section for any N_2 RRS line, or with Eq. (28) and values from Table 2 to calculate the total RRS scattering.

In experiment 2, the slit function encompassed several RRS lines simultaneously. In this case the contribution of individual lines was evaluated using Eq. (48) cna the procedure described

above for CO_2 cross section measurement. The cross section ($F\sigma_{zz}$) and U-values in experiments 1, 2 and 3 at 4880Å differ by more than the estimated error, and increase with slit settings. Such behavior could be produced by a broad background. This possibility was evaluated by observing the RRS spectral region with the cell filled to 700 torr with argon, which exhibits about the same Rayleigh scattering as N_2, but negligible RRS. Although a slight increase in background was observed when the argon was admitted to the cell, the increase was much too small to account for the observed effect. Likewise, the expected widths of RRS lines (ref. 17) are too small to have a significant effect of this type. Exploration of other possibilities has not uncovered a plausible explanation for this small discrepancy.

The results at 647.1 nm are smaller than those at 488.0 nm. This trend is consistent with theoretical expectations which will be discussed subsequently. A simple average of the results for each wavelength yields

$$U(N_2,\ 488.0\ nm) = 7.18 \times 10^{-47} cm^6/sr \pm 8\% \qquad (50)$$

and

$$U(N_2,\ 647.1\ nm) = 6.36 \times 10^{-47} cm^6/sr \pm 8\% \qquad (51)$$

The error estimates have not been decreased as a result of the averages because a dominant portion of each is systematic in origin. The derivation of error estimates for these and subsequent measurements is presented in Appendix C.

The U-values can be used along with information presented previously in this report to calculate particular RRS cross sections. For example, using Eqs. (6), (23) and (28) and (51), and Table 2, we calculate that the cross section for RRS backscattering of 647.1 nm radiation from N_2, summed over Stokes and anti-Stokes bands and over scattered light polarizations, is 4.71×10^{-30} $cm^2/sr \pm 8\%$.

The results given in Eqs. (50) and (51) compare favorably to values calculated from recent precision measurements of the depolarization of the Rayleigh plus RRS band. Rowell, Aval and Barrett (ref. 17) obtain

$$\rho_T = (1.08 \pm 0.01)\%$$

for incident light at 488.0 nm. Their error estimate is derived from the variance in the result of several experiments. Substituting this result into Eq. (33) we obtain $U(N_2, 488.0\ nm) = 7.24 \times 10^{-47}$ cm^6/sr. Similarly, Bridge and Buckingham (ref. 18) obtained

$$\rho_T = 1.018\%$$

for incident light at 632.8 nm. Their result yields $U(N_2, 632.8\ nm) = 6.72 \times 10^{-47} cm^6/sr$.

Table 4. Results for N_2 RRS intensities at 23°C. In this table $(F\sigma_{zz})_A$ is obtained from absolute measurements of laser power and scattering power, X is the ratio of the theoretical Rayleigh cross section to the corresponding experimental result, and $(F\sigma_{zz})_X$ is the product of these two quantities. The quantity $U(N_2,\lambda_o)$ is calculated from $(F\sigma_{zz})_X$ using Eq. 18. The estimated errors for $(F\sigma_{zz})_X$ and $U(N_2,\lambda_o)$ are 8% (See Appendix C). In experiment #1, the entrance slit was narrower than the image of the incident beam on the slit. In this case the results for $(F\sigma_{zz})_A$ and X are misleading; consequently they are omitted in the table.

Exp. #	λ_o	Transition $J \rightarrow J'$	Slits	M	$(F\sigma_{zz})_A \cdot 10^{31}$ (cm^2/sr)	X	$(F\sigma_{zz})_X \cdot 10^{31}$ (cm^2/sr)	$U(N_2,\lambda_o) \cdot 10^{47}$ (cm^6/sr)
1	488.0	6→8	75/150	2.00	----	----	5.57	6.65
2	488.0	6→8	455/1364	2.00	6.48	1.005	6.52	7.78
3	488.0	8→6	200/300	0.85	4.73	0.961	4.55	7.09
4	647.1	8→10	200/400	0.85	1.460	1.082	1.580	6.20
5	647.1	8→6	200/300	0.85	1.278	1.06	1.355	6.52
			300/500	0.85	1.280	1.06	1.357	6.52

Oxygen

The intensities of RRS lines were measured relative to N_2 lines. Values for the ratio $U(O_2,\lambda_o)/U(N_2,\lambda_o)$ and the absolute U-values $U(O_2,\lambda_o)$ were calculated from the observed intensity ratios, using Eqs. (47), (50) and (51). The results are shown in Table 5.

The excellent agreement between results from the several experiments at 647.1 nm probably is due to the relative simplicity of the experimental procedures for these measurements. Averaging the data at 647.1 nm, we obtain for final values

$$U(O_2,\ 488.0\ nm) = 18.69 \times 10^{-47} cm^6/sr \pm 10\% \qquad (52)$$

$$U(O_2,\ 647.1\ nm) = 15.95 \times 10^{-47} cm^6/sr \pm 10\% \qquad (53)$$

The error estimates in Eqs. (52) and (53) apply to the absolute intensity values for O_2. However the realtive (to N_2) RRS intensity for O_2 is measured to better accuracy. For example, using an average of the relative values $U(O_2,\lambda_o)/U(N_2,\lambda_o)$ and Eq. (28) we calculate that the cross sections for RRS scattering of 647.1 nm light from O_2 are 2.50 ± 5% times larger than corresponding cross sections for N_2.

The only previous direct measurement of a RRS line intensity we have found was reported by Weber, et al (ref. 5). They found that the ratio of the N=7 rotational line of O_2, integrated over all angles, was 1.420 of the integrated Rayleigh scattering. Unfortunately they do not give a detailed description of their experimental procedure for this measurement, not an error estimate. However using their value, we obtain from Eq. (8):

$$\frac{8\pi}{3}(F_7\sigma_{zz})_{7\to9}(1+2\rho_{RRS}) = \frac{8\pi}{3}\left(\frac{1}{420}\right)(\sigma_{zz})_{RAY}(1+2\rho_{RAY}) \qquad (54)$$

At 488.0, $(\sigma_{zz})_{RAY}$ for O_2 is computed to be $7.25 \times 10^{-28} cm^2/sr$. Using $\rho_{RRS} = 0.75$ and $\rho_{RAY} = 0.0025$, we obtain $(F_7\sigma_{zz})_{7\to9} = 6.9 \times 10^{-31} cm^2/sr$ from which $U(O_2,\ 488.0) = 8.62 \times 10^{-47}$. Thus their result agrees poorly with out U-values for O_2.

On the other hand, our results are in good agreement with the U-balue calculated from measurement of ρ_T for O_2 at 488.0 nm by Towell et al which yields $U(O_2,\ 488.0\ nm) = 16.47 \times 10^{-47} cm^6/sr$. Also, from the measurement of ρ_T for O_2 at 632.8 nm by Bridge and Buckingham we obtain $16.85 \times 10^{-47} cm^6/sr$.

Carbon Dioxide

The CO_2 RRS intensities were also measured relative to N_2. As mentioned previously, it was not considered desirable to use slit settings narrow enough to resolve separate lines in this spectrum. Therefore, conveniently wide settings were used and the slit function encompassed several CO_2 lines simultaneously.

Table 5. Results for O_2 RRS intensities measured relative to N_2 at 700 torr and 23°C. The U-values for O_2 are calculated using Eqs.(47), (50) and (51) in the text. The estimated relative errors for values of D and the ratio $U(O_2,\lambda_o)/U(N_2,\lambda_o)$ are ±5%. The estimated error in values for $U(O_2,\lambda_o)$ is ±10%.

Exp. #	λ_o (nm)	slits	Transition O_2:N→N'	Transition N_2:J→J'	D	$U(O_2,\lambda_o)/U(N_2,\lambda_o)$	$U(O_2,\lambda_o) \times 10^{47}$ cm^6/sr
3	488.0	200/300	11→9	8→6	3.15	2.605	18.69
4	647.1	200/400	11→9	8→6	3.06	2.520	16.02
6	647.1	200/400	11→9	8→6	3.00	2.470	15.74
			9→11	6→8	3.06	2.535	16.10

Table 6. Results for CO_2 RRS intensity measurements at (23±0.5)°C. U-values were calculated using measured count ratios and Eqs.(47), (50) and (57) in the text. Estimated relative errors are ±10% for the ratios $U(CO_2,\lambda_o)/U(N_2,\lambda_o)$ and ±12% for values of $U(CO_2,\lambda_2)$.

Exp. #	λ_o nm	Slits µm	λ_{CO_2} nm	$N_2: J \to J'$	$U(CO_2,\lambda_o)/U(N_2,\lambda_o)$	$U(CO_2,\lambda_o) \cdot 10^{47}$ cm^6/sr^{-1}
	488.0	200/300	4870	6→4	10.61	76.1
	647.1	300/500	6460	4→2	10.40	66.2

U-values for CO_2 were calculated from the resulting signals for CO_2 and N_2 RRS using Eqs. (49), (50) and (51). The results are shown in Table 6.

The U-values calculated from measurements of ρ_T for CO_2 at 488.0 mm by Rowell et al is 59.2 x 10^{-46} $cm^6 sr^{-1}$, whereas that at 632.8 nm by Bridge and Buckingham yields 61.6 x 10^{-47} cm^6/sr. These results are in fairly good agreement with ours.

Wavelength Dependence of U-values

One of the notable characteristics of the cross section results is that the measured U-values are smaller at 647.1 nm than at 488.0 nm by about 10-15%. This trend is consistent with theoretical expectations. A general quantum-mechanical expression for a cross section σ_{zz} can be put into the form (ref. 19);

$$\sigma_{zz} = (2\pi)^4 (\omega_o - \omega_{fi})^4 (1/hc)^2 \qquad (55)$$

$$(x) \quad \sum_i F_i \sum_f \left| \sum_r (D_z)^*_{rf} (D_z)_{ri} \left(\frac{1}{\omega_{ri} - \omega_o} + \frac{1}{\omega_{rf} + \omega_o} \right) \right|^2$$

Here c denotes the speed of light and h is Planck's constant. The symbol ω_{fi} denotes $\omega_f - \omega_i$, where $hc\omega_f$ is the energy of the f-state. Other frequency functions are similarly defined. The symbol $(D_z)_{ri}$ represents the matrix element of the x component of the dipole moment between intermediate state r and initial state i; $(D_z)_{rf}$ is similarly defined and the superscript asterisk denotes complex conjugate. The sum over final states extends over all final states with the proper energy to product the observed scattering from the initial state i. The sum over initial states extends over all states which lead to the observed scattering; weighted by the population fraction F_i. It is useful to separate the rotational dependence of the molecule state functions using the Born-Oppenheimer approximation. For pure RRS from ground state SLM, the sums over i and f involve only rotational states. Furthermore, away from resonance the dependence of the frequency factors ω_{ri} and ω_{rf} on rotation can be ignored to a good approximation. Then the rotational part of the intermediate states can be summed using closure, and the dependence of the cross section on rotation can be extracted in the form of Placzek-Teller coefficients $b_{J \to J}$. Separating the $(\omega_o - \omega_{fi})^4$ and F_i factors of the cross section, as in Eq. 16, we find for the U-values

$$U \propto \sum_r \left| (D_z)_{ri} \right|^2 \frac{\omega_{ri}^2}{\omega_{ri}^2 - \omega_0^2} \qquad (56)$$

In this equation the symbols i and r denote only the vibrational and electronic components of the state functions.

Likewise, from a quantum-mechanical expression for the refractive index n of a gas, we find

$$n-1 \propto \sum_r \left|(D_z)_{ri}\right|^2 \frac{\omega_{ri}}{\omega_{ri}^2-\omega_o^2} \tag{57}$$

Thus, within these approximations the frequency dependence of U and $(n-1)^2$ should be the same; i.e.

$$U \propto (n-1)^2 \tag{58}$$

Equation (58) should predict the frequency or wavelength dependence of the U-values to good accuracy away from dominant resonances. In particular, for N_2 the ratio

$$\frac{(n-1)_{6471}}{(n-1)_{4880}} \simeq .988 \tag{59}$$

Thus $U(N_2, 647.1)$ should be about 2.2% smaller than $U(N_2, 488.0)$. Although the observed frequency dependence is larger, it is in the same direction and the difference is well within experimental error.

DEPOLARIZATION MEASUREMENTS: PROCEDURE AND RESULTS

The depolarizations of various RRS lines were measured by rotating the polarization of the incident beam. Two incident beam polarization states were involved:

1. UR(unrotated): polarization perpendicular to monochromator axis
2. R(rotated): polarization parallel to monochromator axis

With the incident beam in polarization state UR, the scattered light intensities with polarization perpendicular and parallel to grating grooves are, respectively, $I_\perp$, and $\rho I_\perp$. In the second

state, the scattered light intensity with each polarization is ρI_z. Therefore, the ratio of signal count rates obtained with the two incident beam polarization states is given by

$$\frac{C_1}{C_2} = \frac{I_\perp \rho R_\perp + I_\parallel \rho R_\parallel}{I_\perp R_\perp + I_\perp \rho R_\parallel} = \rho \left(\frac{1+\alpha}{1+\rho\alpha}\right) \tag{60}$$

where α is defined by Eq. 39. Solving this equation for ρ, we obtain

$$\rho = \frac{C_2/C_1}{1+\alpha(1-C_2/C_1)} \tag{61}$$

The ratios C_2/C_1 for a number of RRS lines for each gas were measured at 23°C. The depolarization values calculated from these measurements are shown in Table 7. The results at 488.0 nm are consistently lower than the theoretical value of 3/4. The average of these results is 0.721, and for a majority the deviation from 3/4 is slightly larger than the estimated error. On the other hand, the depolarization measurements at 647.1 nm conform quite well to theoretical expectations. The average of these results is 0.750 and only one of six differs from 3/4 by more than the estimated error.

COMPARISON OF LINE INTENSITIES IN EXPERIMENTAL AND THEORETICAL RRS SPECTRA

Detailed RRS spectra of N_2, O_2 and CO_2 were taken for incident light at 488.0 nm and 647.1 nm. The purpose of these experiments was to examine the agreement between experimental and theoretical line intensities. For each gas these spectra were obtained at several different temperatures. (Nominally 23°C, 75°C, and 125°C). Incident beam polarization states UR and R were both employed in these measurements. The various combination of these parameters for which spectra were obtained are shown in Tables 8 and 9.

Table 7. Depolarization of RRS lines. The transitions shown for CO_2 are at the center of the observed spectral region, which encompassed several lines.

Exp. #	λ_o	Gas	Transition	ρ	Error Estimate
3	4880	N_2	8→6	.742	±.054
			10→8	.739	±.058
		O_2	13→11	.707	±.030
			15→13	.713	±.035
		CO_2	21→19	.714	±.027
			27→25	.713	±.030
4	6471	N_2	10→8	.684	±.063
			8→6	.758	±.069
		O_2	13→11	.770	±.040
			11→9	.786	±.038
		CO_2	19→17	.743	±.024
			23→21	.770	±.026

Table 8. Experimental parameters for RRS spectra intensity measurements at 488.0 nm. The slit settings for all experiments listed in this table were 90/500/180μm.

Experiment No.	Gas	Nominal Temp.	Incident Beam Polarization
090172C	N_2	23°C	UR
090172D	N_2	23°C	R
090172A	O_2	23°C	UR
090172B	O_2	23°C	R
090572C	CO_2	23°C	UR
090572B	CO_2	23°C	R
090672B	N_2	125°C	UR
090672C	N_2	125°C	R
090772A	N_2	75°C	UR
090772C	N_2	75°C	R

Table 9. Experimental parameters for RRS spectra intensity measurements at 647.1 nm. The slit settings for all experiments listed in this table were 130/500/260μm.

Experiment No.	Gas	Nominal Temp.	Incident Beam Polarization
091472B	N_2	23°C	UR
091462C	O_2	23°C	UR
091472D	CO_2	23°C	UR
091572A	N_2	75°C	UR
091572B	O_2	75°C	UR
091872A	CO_2	75°C	UR
091872D	CO_2	125°C	UR
091872C	CO_2	125°C	R
091972A	N_2	125°C	UR
091972B	N_2	125°C	R
091972D	O_2	125°C	UR
091972C	O_2	125°C	R

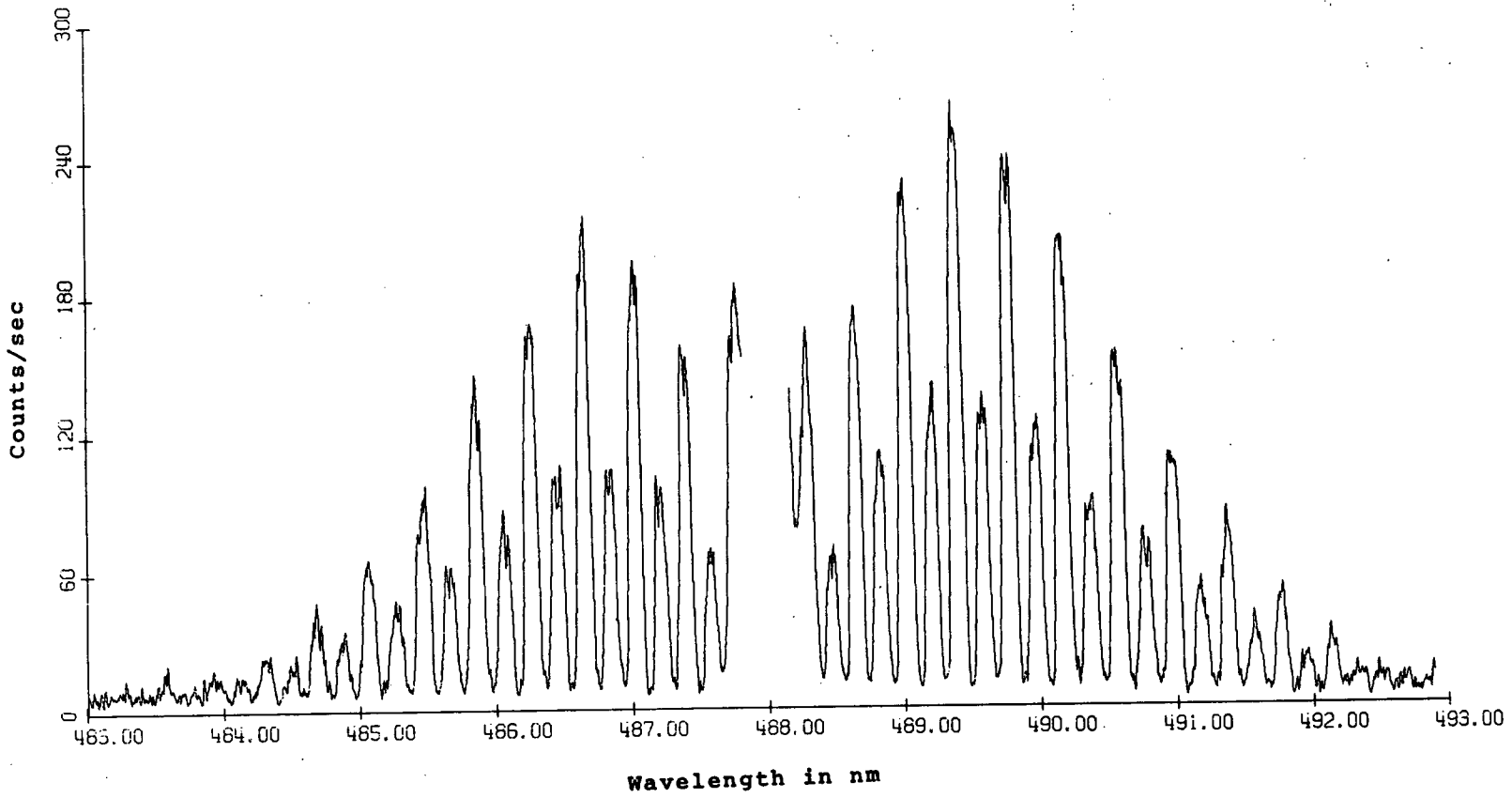

Figure 3. Rotational Raman spectrum of N_2 at 23°C excited by incident light at 488.0 nm. Experiment no. 090172C.

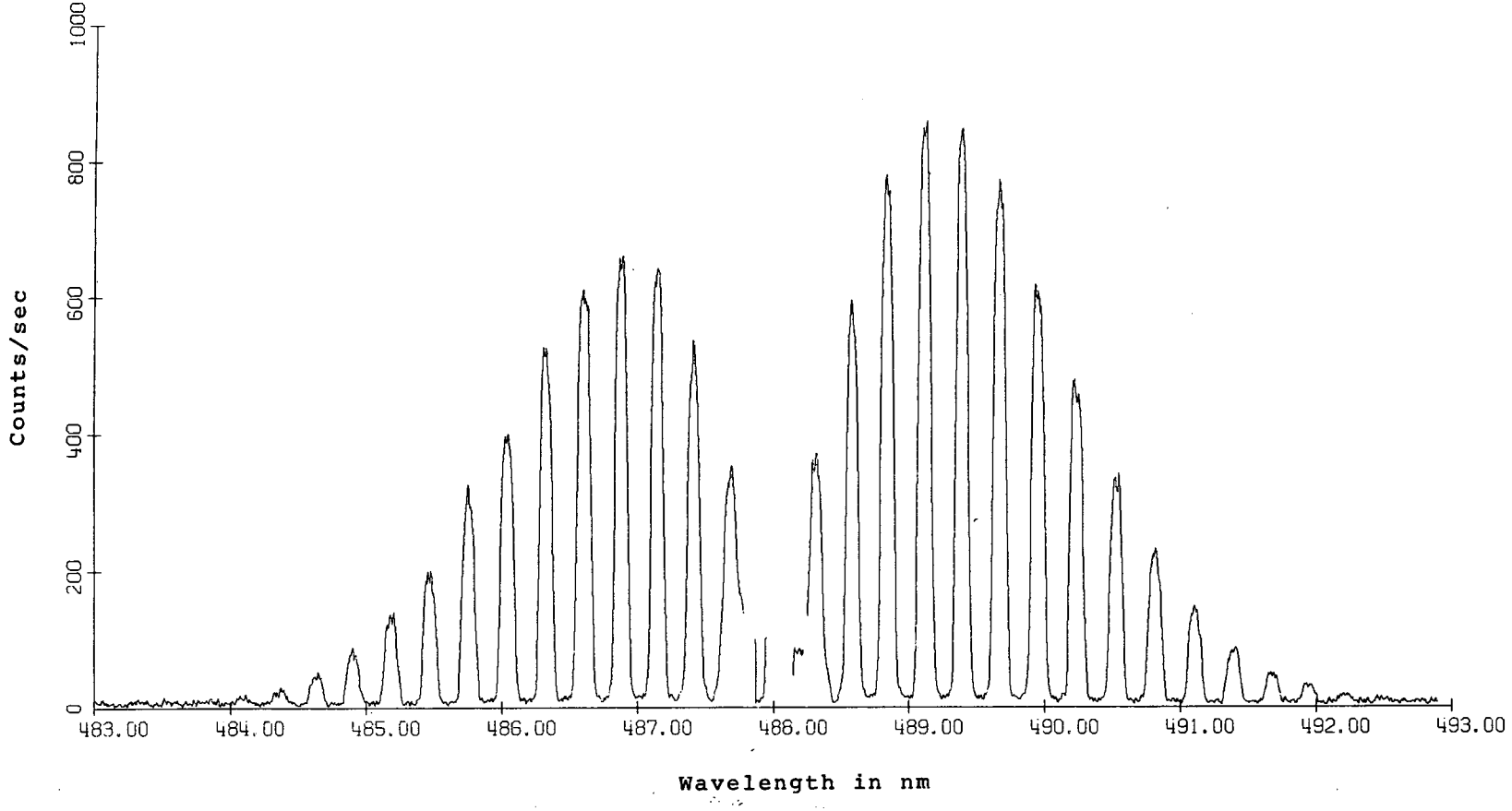

Figure 4. Rotational Raman spectrum of O_2 at 23°C excited by incident light at 488.0 nm. Experiment no. 090172A.

The data obtained in these experiments were transferred to computer files via paper tape records. From these files the data set was smoothed by an appropriate averaging function and then, when desired, plotted on a digital x-y recorder for display. Example results for N_2 and O_2 RRS are shown in Figs. 3 and 4.

In the N_2 and O_2 spectra individual lines were resolved, whereas in the case of CO_2, the slit function encompassed several lines. Consequently, different procedures were used to analyze the two types of data.

Nitrogen and Oxygen

Experimental signal strengths $C_{J\to J'}$, were obtained by a hand average of the net detector count over five - one second periods at the center of the flat-topped portion of each peak. Since individual lines were resolved in these spectra, the background count for each line was determined from the minimum counts between the lines.

The corresponding theoretical count rates $T_{J\to J'}$, are given by a product of expressions for the line intensity, Eqs.(11) and (15), and corresponding monochromator response. Thus for the incident beam polarization state UR, from Eqs. 16 and 41

$$T^{UR}_{J\to J'} \propto P_o N F_J b_{J\to J'}(\omega_o-\omega_{J\to J'})^4 U R_\perp (1+\rho_q\alpha) \qquad (62)$$

Substituting for $R_\perp$ from Eq.(40), and setting

$$N = N_o \left(\frac{p}{760\ \text{torr}}\right)\left(\frac{273°K}{\theta}\right) \qquad (63)$$

we obtain

$$T^{UR}_{J\to J'} = G\left[P_o \left(\frac{p}{760\ \text{torr}}\right)\left(\frac{273°K}{\theta}\right) F_J b_{J\to J'}(\omega_o-\omega_{J\to J'})^4 U\ (x)\frac{I\lambda\Delta}{Co}\left(\frac{1+\rho_q\gamma}{1+\gamma}\right)\right] \qquad (64)$$

Here G is the product of those factors which are effectively independent of wavelength, polarization and gas state.

For the incident beam polarization state R, the polarization components of the scattered light intensity are related theoretically by

$$I_X^R = I_X^R = \rho_q I_Z^{UR} = 0.75\ I_Z^{UR} \tag{65}$$

Consequently, the depolarization of the observed scattered light is unity. In this case, ρ must be replaced by unity in Eq.(64), and

$$T^R_{J\to J'} = G[P_o(0.75)(\frac{p}{760\ \text{torr}})(\frac{273°K}{\Theta})F_J{}^b{}_{J\to J'}(\omega-\omega_{J\to J'})^4 U(\frac{I_\lambda \Delta}{Co})] \tag{66}$$

Theoretical and experimental results for each experiment were compared by calculating the product of factors within the brackets in Eq.(64) and (66) and then multiplying the product by a normalization constant G chosen to produce the best mean square fit with experimental data. The innermost lines were not considered in this fit because of substantial uncertainty in the background associated with them. Results are shown in Tables 10 through 25, which include normalization constants, the experimental count rate, theoretical count rate, deviation (theoretical-experimental count rates), and ratio of this deviation to the theoretical S.D. The theoretical S.D. is calculated from

$$(S.D.)_{J\to J'} = \sqrt{T_{J\to J'}/5} \tag{67}$$

where the factor 5 comes from the fact that 5 counts were averaged to produce the experiment data sets.

These tables provide two significant types of comparison:

1. the variation of the normalization constant from table to table;
2. the variation of line intensities within a table.

Since all of the expected variation in count rate with incident beam power, polarization and wavelength, and gas type, temperature and pressure are included in the un-normalized theoretical spectra, ideally the normalization constants should all be equal within a very small statistical error. Actually, these constants vary from 63.4 to 44.6. This variation probably arises from one or both of the following factors:

1. variations in system sensitivity from day to day.
2. changes in alignment and/or beam profile from one experiment to the next.

There are several possible sources of variations in system sensitivity. Following experiment 090772C the Hamner pulse

TABLE 10. COMPARISON OF THEORETICAL AND EXPERIMENTAL RRS LINE INTENSITIES.

EXPERIMENT NO.	=090172C
GAS	=N2
WAVELENGTH IN NM	=488.0
POLARIZATION	=UR
TEMP. IN C	=23
PRESSURE IN TORR	=704.3
POWER IN WATTS	=.675
U-VALUE*10**47	=7.17
NORM. CONST.	= 59.9

J	EXPERIMENTAL LINE INTENSITY	THEORETICAL LINE INTENSITY	THEORETICAL % STAND. DEV.	RATIO: DEV. TO STAND.DEV.
STOKES				
0	147.00	66.17	5.50	22.22
1	53.80	58.48	5.85	-1.37
2	161.60	160.90	3.53	0.16
3	101.20	98.50	4.51	0.61
4	217.00	223.93	2.99	-1.04
5	124.20	120.49	4.07	0.76
6	244.60	248.08	2.84	-0.47
7	120.80	122.95	4.03	-0.43
8	220.40	235.67	2.91	-2.22
9	114.80	109.51	4.27	1.13
10	197.60	197.77	3.18	-0.03
11	82.40	86.91	4.80	-1.08
12	144.60	148.85	3.67	-0.78
13	58.80	62.16	5.67	-0.95
14	99.60	101.35	4.44	-0.39
15	44.80	40.34	7.04	1.57
16	73.00	62.77	5.64	2.89
17	30.40	23.67	9.15	2.99
18	40.40	35.49	7.51	1.84
19	15.80	12.91	12.45	1.80
20	22.80	18.37	10.43	2.31
ANTISTOKES				
2	163.80	62.19	5.67	28.81
3	60.80	52.74	6.16	2.48
4	138.80	139.22	3.79	-0.08
5	83.90	81.77	4.95	0.50
6	180.60	178.38	3.35	0.37
7	91.80	92.09	4.66	-0.07
8	196.20	181.93	3.32	2.37
9	87.20	86.51	4.81	0.17
10	157.20	159.11	3.55	-0.34
11	76.00	70.93	5.31	1.34
12	131.60	122.92	4.03	1.75
13	51.60	51.83	6.21	-0.07
14	84.40	85.17	4.85	-0.19
15	37.40	34.13	7.66	1.25
16	57.00	53.38	6.12	1.11
17	25.60	20.39	9.90	2.58
18	35.20	30.44	8.11	1.93
19	12.00	11.10	13.48	0.60
20	15.60	15.84	11.24	-0.14

TABLE II. COMPARISON OF THEORETICAL AND EXPERIMENTAL RRS LINE INTENSITIES.

EXPERIMENT NO.	=090172D
GAS	=N2
WAVELENGTH IN NM	=488.0
POLARIZATION	=R
TEMP. IN C	=23
PRESSURE IN TORR	=704.3
POWER IN WATTS	=.648
U-VALUE*10**47	=7.17
NORM. CONST.	= 63.4

J	EXPERIMENTAL LINE INTENSITY	THEORETICAL LINE INTENSITY	THEORETICAL % STAND. DEV.	RATIO: DEV. TO STAND.DEV.
STOKES				
0	59.00	58.11	5.87	0.26
1	47.40	51.35	6.24	-1.23
2	146.80	141.26	3.76	1.04
3	92.20	86.46	4.81	1.38
4	190.00	196.56	3.19	-1.05
5	101.20	105.75	4.35	-0.99
6	204.20	217.70	3.03	-2.05
7	109.80	107.88	4.31	0.41
8	202.20	206.76	3.11	-0.71
9	97.80	96.06	4.56	0.40
10	177.80	173.48	3.40	0.73
11	79.60	76.22	5.12	0.87
12	132.40	130.53	3.91	0.37
13	57.40	54.50	6.06	0.88
14	84.80	88.85	4.74	-0.96
15	35.60	35.37	7.52	0.09
16	52.20	55.02	6.03	-0.85
17	22.40	20.92	9.78	0.73
18	32.00	31.10	8.02	0.36
19	12.00	11.31	13.30	0.46
20	15.20	16.09	11.15	-0.50
ANTISTOKES				
2	65.80	54.63	6.05	3.38
3	42.40	46.33	6.57	-1.29
4	126.20	122.33	4.04	0.78
5	70.40	71.86	5.28	-0.38
6	147.60	156.77	3.57	-1.64
7	80.80	80.94	4.97	-0.04
8	166.80	159.92	3.54	1.22
9	80.00	76.06	5.13	1.01
10	147.20	139.89	3.78	1.38
11	66.20	62.38	5.66	1.08
12	112.60	108.10	4.30	0.97
13	49.00	45.58	6.62	1.13
14	76.40	74.92	5.17	0.38
15	32.40	30.02	8.16	0.97
16	47.60	46.97	6.53	0.21
17	21.20	17.94	10.56	1.72
18	31.60	26.78	8.64	2.08
19	9.60	9.77	14.31	-0.12
20	16.40	13.94	11.98	1.47

TABLE 12. COMPARISON OF THEORETICAL AND EXPERIMENTAL RRS LINE INTENSITIES.

EXPERIMENT NO.	=090172A
GAS	=02
WAVELENGTH IN NM	=488.0
POLARIZATION	=UR
TEMP. IN C	=23
PRESSURE IN TORR	=708.7
POWER IN WATTS	=.690
U-VALUE*10**47	=18.69
NORM. CONST.	= 60.7

J	EXPERIMENTAL LINE INTENSITY	THEORETICAL LINE INTENSITY	THEORETICAL % STAND. DEV.	RATIO: DEV. TO STAND.DEV.
STOKES				
1	347.20	344.23	2.41	0.36
3	575.80	595.47	1.83	-1.80
5	756.40	764.71	1.62	-0.67
7	836.40	837.36	1.55	-0.07
9	834.40	818.01	1.56	1.28
11	750.00	727.85	1.66	1.84
13	600.60	596.57	1.83	0.37
15	451.00	453.52	2.10	-0.26
17	318.20	321.21	2.50	-0.38
19	220.00	212.60	3.07	1.13
21	136.60	131.79	3.90	0.94
23	76.60	76.64	5.11	-0.01
25	42.40	41.87	6.91	0.18
27	24.60	21.50	9.64	1.49
ANTISTOKES				
3	325.40	319.58	2.50	0.73
5	511.40	520.93	1.96	-0.93
7	627.40	630.39	1.73	-0.27
9	644.60	650.45	1.75	-0.51
11	594.80	598.75	1.83	-0.36
13	510.20	502.01	2.00	0.82
15	386.20	387.72	2.27	-0.17
17	305.40	277.74	2.68	3.71
19	185.80	185.35	3.28	0.07
21	124.80	115.60	4.16	1.91
23	76.60	67.52	5.44	2.47
25	39.60	37.00	7.35	0.96
27	20.60	19.04	10.25	0.80

TABLE 13. COMPARISON OF THEORETICAL AND EXPERIMENTAL RRS LINE INTENSITIES.

EXPERIMENT NO.	=090172B
GAS	=02
WAVELENGTH IN NM	=488.0
POLARIZATION	=R
TEMP. IN C	=23
PRESSURE IN TORR	=708.7
POWER IN WATTS	=.675
U-VALUE*10**47	=18.69
NORM. CONST.	= 60.4

J	EXPERIMENTAL LINE INTENSITY	THEORETICAL LINE INTENSITY	THEORETICAL % STAND. DEV.	RATIO: DEV. TO STAND.DEV.
STOKES				
1	249.00	290.16	2.63	-5.40
3	483.00	501.86	2.00	-1.88
5	653.60	644.39	1.76	0.81
7	702.20	705.50	1.68	-0.28
9	680.80	689.08	1.70	-0.71
11	624.40	613.02	1.81	1.03
13	514.00	502.37	2.00	1.16
15	397.40	381.85	2.29	1.78
17	275.40	270.40	2.72	0.68
19	187.80	178.94	3.34	1.48
21	121.20	110.91	4.25	2.19
23	69.80	64.49	5.57	1.48
ANTISTOKES				
3	237.20	269.50	2.72	-4.40
5	421.60	439.37	2.13	-1.90
7	514.40	531.77	1.94	-1.68
9	545.60	548.78	1.91	-0.30
11	502.40	505.24	1.99	-0.28
13	422.40	423.68	2.17	-0.14
15	331.00	327.27	2.47	0.46
17	230.20	234.47	2.92	-0.62
19	157.60	156.51	3.57	0.20
21	102.60	97.62	4.53	1.13
23	56.20	57.03	5.92	-0.25
25	34.00	31.26	8.00	1.10

TABLE 14. COMPARISON OF THEORETICAL AND EXPERIMENTAL RRS LINE INTENSITIES.

EXPERIMENT NO.	=090672B
GAS	=N2
WAVELENGTH IN NM	=486.0
POLARIZATION	=UR
TEMP. IN C	=123
PRESSURE IN TORR	=711.9
POWER IN WATTS	=.620
U-VALUE*10**47	=7.17
NORM. CONST.	= 62.6

J	EXPERIMENTAL LINE INTENSITY	THEORETICAL LINE INTENSITY	THEORETICAL % STAND. DEV.	RATIO: DEV. TO STAND.DEV.
STOKES				
0	101.20	35.51	7.51	24.65
1	31.20	31.53	7.96	-0.13
2	80.40	87.63	4.78	-1.73
3	52.00	54.45	6.06	-0.74
4	117.20	126.29	3.98	-1.81
5	69.20	69.67	5.36	-0.13
6	146.80	147.79	3.68	-0.18
7	81.40	75.85	5.14	1.43
8	149.60	151.29	3.64	-0.31
9	73.80	73.53	5.22	0.07
10	141.40	139.58	3.79	0.35
11	71.20	64.79	5.56	1.78
12	121.60	117.80	4.12	0.78
13	54.00	52.49	6.17	0.47
14	96.80	91.76	4.67	1.18
15	41.40	39.36	7.13	0.73
16	69.00	66.32	5.49	0.74
17	28.80	27.45	8.54	0.58
18	46.00	44.65	6.69	0.45
19	18.60	17.85	10.59	0.40
20	21.80	28.07	8.44	-8.64
21	11.80	10.85	13.58	0.64
22	19.20	16.51	11.01	1.48
ANTISTOKES				
2	109.20	33.87	7.68	28.94
3	24.60	29.15	8.28	-1.89
4	77.40	78.52	5.05	-0.28
5	45.40	47.28	6.50	-0.61
6	109.40	106.27	4.34	0.68
7	55.60	56.81	5.93	-0.36
8	112.80	116.80	4.14	-0.83
9	58.00	58.09	5.87	-0.03
10	116.80	112.29	4.22	0.95
11	57.00	52.88	6.15	1.27
12	95.20	97.28	4.53	-0.47
13	42.60	43.76	6.76	-0.39
14	75.20	77.11	5.09	-0.49
15	33.60	33.29	7.75	0.12
16	56.60	56.41	5.95	0.06
17	24.20	23.45	9.24	0.35
18	41.80	38.29	7.23	1.27
19	16.00	15.35	11.41	0.37
20	24.40	24.20	9.09	0.09
21	9.40	9.38	14.60	0.02
22	15.20	14.29	11.83	0.54

TABLE 15. COMPARISON OF THEORETICAL AND EXPERIMENTAL RRS LINE INTENSITIES.

EXPERIMENT NO.	=090672C
GAS	=N2
WAVELENGTH IN NM	=488.0
POLARIZATION	=R
TEMP. IN C	=123
PRESSURE IN TORR	=711.9
POWER IN WATTS	=.605
U-VALUE*10**47	=7.17
NORM. CONST.	= 59.5

J	EXPERIMENTAL LINE INTENSITY	THEORETICAL LINE INTENSITY	THEORETICAL % STAND. DEV.	RATIO: DEV. TO STAND.DEV.
STOKES				
0	32.80	28.50	8.38	1.80
1	20.60	25.31	8.89	-2.09
2	68.80	70.33	5.33	-0.41
3	44.00	43.69	6.77	0.10
4	103.00	101.33	4.44	0.37
5	57.60	55.89	5.98	0.51
6	124.00	118.55	4.11	1.12
7	60.80	60.83	5.73	-0.01
8	113.40	121.33	4.06	-1.61
9	54.40	58.96	5.82	-1.33
10	110.80	111.91	4.23	-0.23
11	46.00	51.94	6.21	-1.84
12	94.60	94.43	4.60	0.04
13	44.20	42.07	6.90	0.74
14	70.80	73.53	5.22	-0.71
15	31.40	31.54	7.96	-0.06
16	57.00	53.14	6.14	1.19
17	24.20	21.99	9.54	1.06
18	30.40	35.76	7.48	-2.00
19	16.40	14.30	11.83	1.24
20	19.60	22.47	9.43	-1.36
21	10.00	8.69	15.17	1.00
22	19.40	13.21	12.30	3.81
ANTISTOKES				
2	40.40	27.20	8.58	5.66
3	27.00	23.41	9.24	1.66
4	66.60	63.06	5.63	1.00
5	35.00	37.98	7.26	-1.08
6	85.00	85.37	4.84	-0.09
7	43.80	45.64	6.62	-0.61
8	97.20	93.84	4.62	0.77
9	51.00	46.68	6.55	1.41
10	92.00	90.24	4.71	0.41
11	44.80	42.50	6.86	0.79
12	80.80	78.20	5.06	0.66
13	38.00	35.18	7.54	1.06
14	61.00	62.00	5.68	-0.28
15	21.60	26.77	8.64	-2.24
16	46.80	45.36	6.64	0.48
17	18.20	18.86	10.30	-0.34
18	31.20	30.80	8.06	0.16
19	11.60	12.35	12.72	-0.48
20	20.80	19.47	10.13	0.67
21	7.40	7.54	16.28	-0.12
22	14.40	11.50	13.19	1.91

TABLE 16. CØMPARISØN ØF THEØRETICAL AND EXPERIMENTAL RRS LINE INTENSITIES.

EXPERIMENT NØ.	=090772A
GAS	=N2
WAVELENGTH IN NM	=488.0
PØLARIZATIØN	=UR
TEMP. IN C	=75
PRESSURE IN TØRR	=720.8
PØWER IN WATTS	=.630
U-VALUE*10**47	=7.17
NØRM. CØNST.	= 50.4

J	EXPERIMENTAL LINE INTENSITY	THEØRETICAL LINE INTENSITY	THEØRETICAL % STAND. DEV.	RATIØ: DEV. TØ STAND.DEV.
STØKES				
0	91.40	38.51	7.21	19.06
1	31.40	34.13	7.66	-1.04
2	90.80	94.45	4.60	-0.84
3	55.00	58.32	5.86	-0.97
4	135.00	134.15	3.86	0.16
5	65.80	73.23	5.23	-1.94
6	142.20	153.44	3.61	-2.03
7	73.00	77.61	5.08	-1.17
8	141.60	152.25	3.62	-1.93
9	71.20	72.62	5.25	-0.37
10	128.20	135.02	3.85	-1.31
11	61.60	61.26	5.71	0.10
12	100.40	108.65	4.29	-1.77
13	45.40	47.12	6.52	-0.56
14	75.20	80.01	5.00	-1.20
15	29.20	33.27	7.75	-1.58
16	52.20	54.22	6.07	-0.61
17	20.20	21.66	9.61	-0.70
18	33.80	33.94	7.68	-0.05
19	10.60	13.04	12.38	-1.51
20	15.00	19.68	10.08	-2.36
21	9.80	7.28	16.57	2.09
ANTISTØKES				
2	113.40	36.51	7.40	28.46
3	39.40	31.23	8.00	3.27
4	91.20	83.40	4.90	1.91
5	52.40	49.70	6.34	0.86
6	122.60	110.33	4.26	2.61
7	64.80	58.13	5.87	1.96
8	132.60	117.54	4.13	3.11
9	65.20	57.37	5.90	2.31
10	113.60	108.62	4.29	1.07
11	56.40	50.00	6.32	2.02
12	92.80	89.72	4.72	0.73
13	43.20	39.28	7.14	1.40
14	73.80	67.24	5.45	1.79
15	33.60	28.14	8.43	2.30
16	56.60	46.11	6.59	3.45
17	18.00	18.50	10.40	-0.26
18	35.80	29.11	8.29	2.77
19	12.20	11.22	13.35	0.65
20	16.00	16.97	10.86	-0.53
21	7.00	6.29	17.83	0.63
22	11.20	9.16	14.78	1.51

TABLE 17. COMPARISON OF THEORETICAL AND EXPERIMENTAL RRS LINE INTENSITIES.

EXPERIMENT NO.	=090772C
GAS	=N2
WAVELENGTH IN NM	=488.0
POLARIZATION	=R
TEMP. IN C	=76
PRESSURE IN TORR	=720.8
POWER IN WATTS	=.608
U-VALUE*10**47	=7.17
NORM. CONST.	= 59.8

J	EXPERIMENTAL LINE INTENSITY	THEORETICAL LINE INTENSITY	THEORETICAL % STAND. DEV.	RATIO: DEV. TO STAND.DEV.
STOKES				
0	39.20	38.10	7.25	0.40
1	27.40	33.76	7.70	-2.45
2	90.60	93.43	4.63	-0.66
3	58.20	57.69	5.89	0.15
4	134.20	132.67	3.88	0.30
5	67.00	72.42	5.26	-1.42
6	158.20	151.72	3.63	1.18
7	77.20	76.73	5.11	0.12
8	139.60	150.51	3.65	-1.99
9	69.20	71.78	5.28	-0.68
10	138.60	133.45	3.87	1.00
11	55.40	60.54	5.75	-1.48
12	110.80	107.35	4.32	0.74
13	48.20	46.55	6.55	0.54
14	80.80	79.04	5.03	0.44
15	29.00	32.86	7.80	-1.51
16	57.80	53.55	6.11	1.30
17	27.60	21.39	9.67	3.00
18	34.80	33.51	7.73	0.50
19	10.20	12.88	12.46	-1.67
20	15.20	19.42	10.15	-2.14
ANTISTOKES				
2	39.00	36.13	7.44	1.07
3	30.20	30.91	8.04	-0.29
4	83.20	82.57	4.92	0.16
5	46.00	49.21	6.37	-1.02
6	102.40	109.25	4.28	-1.47
7	53.40	57.57	5.89	-1.23
8	118.80	116.42	4.14	0.49
9	58.00	56.83	5.93	0.35
10	114.40	107.61	4.31	1.46
11	51.60	49.54	6.35	0.65
12	87.00	88.91	4.74	-0.45
13	38.00	38.93	7.17	-0.33
14	66.00	66.64	5.48	-0.18
15	30.20	27.89	8.47	0.98
16	43.80	45.72	6.61	-0.63
17	20.60	18.35	10.44	1.18
18	32.00	28.86	8.32	1.31
19	13.20	11.13	13.41	1.39
20	16.60	16.83	10.90	-0.12

TABLE 18. COMPARISON OF THEORETICAL AND EXPERIMENTAL RRS LINE INTENSITIES.

EXPERIMENT NO.	=091472C
GAS	=02
WAVELENGTH IN NM	=647.1
POLARIZATION	=UR
TEMP. IN C	=23
PRESSURE IN TORR	=723.9
POWER IN WATTS	=.323
U-VALUE*10**47	=15.95
NORM. CONST.	= 44.6

J	EXPERIMENTAL LINE INTENSITY	THEORETICAL LINE INTENSITY	THEORETICAL % STAND. DEV.	RATIO: DEV. TO STAND.DEV.
STOKES				
1	78.00	103.54	4.40	-5.61
3	171.60	177.95	3.35	-1.06
5	217.60	227.05	2.97	-1.40
7	248.60	247.01	2.85	0.23
9	247.40	239.76	2.89	1.10
11	205.80	211.97	3.07	-0.95
13	171.80	172.63	3.40	-0.14
15	135.60	130.40	3.92	1.02
17	96.20	91.78	4.67	1.03
19	57.60	60.36	5.76	-0.80
21	39.40	37.18	7.33	0.81
23	22.80	21.49	9.65	0.63
25	14.40	11.67	13.09	1.79
ANTISTOKES				
3	75.60	97.72	4.52	-5.00
5	156.00	160.35	3.53	-0.77
7	186.00	195.34	3.20	-1.49
9	207.00	202.90	3.14	0.64
11	194.20	188.03	3.26	1.01
13	163.20	158.72	3.55	0.80
15	125.00	123.42	4.03	0.32
17	90.20	89.01	4.74	0.28
19	69.20	59.81	5.76	2.71
21	45.80	37.56	7.30	3.01
23	24.00	22.09	9.51	0.91
25	17.80	12.19	12.81	3.59

TABLE 19. CØMPARISØN ØF THEØRETICAL AND EXPERIMENTAL RRS LINE INTENSITIES.

EXPERIMENT NØ.	=091472B
GAS	=N2
WAVELENGTH IN NM	=647.1
PØLARIZATIØN	=UR
TEMP. IN C	=23
PRESSURE IN TØRR	=723.9
PØWER IN WATTS	=.323
U-VALUE*10**47	=6.36
NØRM. CØNST.	= 51.3

J	EXPERIMENTAL LINE INTENSITY	THEØRETICAL LINE INTENSITY	THEØRETICAL % STAND. DEV.	RATIØ: DEV. TØ STAND.DEV.
STØKES				
0	20.00	24.85	8.97	-2.17
1	20.40	21.86	9.57	-0.70
2	57.20	59.87	5.78	-0.77
3	33.40	36.49	7.40	-1.14
4	81.20	82.58	4.92	-0.34
5	42.40	44.23	6.72	-0.62
6	83.80	90.67	4.70	-1.61
7	44.20	44.74	6.69	-0.18
8	82.40	85.37	4.84	-0.72
9	44.20	39.49	7.12	1.68
10	78.80	71.01	5.31	2.07
11	36.40	31.07	8.02	2.14
12	49.80	52.97	6.14	-0.98
13	23.20	22.03	9.53	0.56
14	40.40	35.75	7.48	1.74
15	16.00	14.17	11.88	1.09
16	22.40	21.95	9.55	0.21
17	9.80	8.31	15.51	1.16
ANTISTØKES				
2	22.20	23.68	9.19	-0.68
3	20.40	20.17	9.96	0.12
4	50.60	53.49	6.11	-0.88
5	35.20	31.56	7.96	1.45
6	63.80	69.18	5.38	-1.45
7	38.00	35.88	7.47	0.79
8	73.40	71.21	5.30	0.58
9	34.80	34.02	7.67	0.30
10	66.20	62.87	5.64	0.94
11	26.80	28.16	8.43	-0.57
12	48.40	49.03	6.39	-0.20
13	25.00	20.77	9.81	2.07
14	36.00	34.30	7.64	0.65
15	17.40	13.81	12.04	2.16
16	26.20	21.70	9.60	2.16
17	9.40	8.33	15.50	0.83
18	14.80	12.49	12.65	1.46

TABLE 20. COMPARISON OF THEORETICAL AND EXPERIMENTAL RRS LINE INTENSITIES.

EXPERIMENT NO.	=091572A
GAS	=N2
WAVELENGTH IN NM	=647.1
POLARIZATION	=UR
TEMP. IN C	=75
PRESSURE IN TORR	=723.6
POWER IN WATTS	=.320
U-VALUE*10**47	=6.36
NORM. CONST.	= 45.6

J	EXPERIMENTAL LINE INTENSITY	THEORETICAL LINE INTENSITY	THEORETICAL % STAND. DEV.	RATIO: DEV. TO STAND.DEV.
STOKES				
0	18.60	15.84	11.24	1.55
1	11.80	13.98	11.96	-1.30
2	37.00	38.51	7.21	-0.54
3	22.60	23.67	9.19	-0.49
4	51.20	54.21	6.07	-0.91
5	34.20	29.46	8.24	1.95
6	62.80	61.45	5.71	0.39
7	28.60	30.94	8.04	-0.94
8	61.80	60.43	5.75	0.39
9	28.20	28.70	8.35	-0.21
10	50.80	53.12	6.14	-0.71
11	23.60	24.00	9.13	-0.18
12	41.80	42.37	6.87	-0.20
13	20.00	18.29	10.46	0.89
14	29.20	30.93	8.04	-0.70
15	13.80	12.80	12.50	0.62
16	24.20	20.78	9.81	1.68
17	10.60	8.26	15.56	1.82
ANTISTOKES				
2	15.20	15.23	11.46	-0.02
3	14.60	13.09	12.36	0.94
4	33.00	35.11	7.55	-0.80
5	20.60	21.02	9.75	-0.21
6	46.80	46.88	6.53	-0.03
7	27.80	24.82	8.98	1.34
8	47.40	50.41	6.30	-0.95
9	26.00	24.72	8.99	0.57
10	52.80	47.03	6.52	1.88
11	23.80	21.75	9.59	0.98
12	37.80	39.21	7.14	-0.51
13	18.40	17.25	10.77	0.62
14	32.40	29.67	8.21	1.12
15	14.60	12.48	12.66	1.34
16	14.00	20.54	9.87	-3.23
17	7.40	8.28	15.54	-0.69
18	13.20	13.09	12.36	0.07

TABLE 21. COMPARISON OF THEORETICAL AND EXPERIMENTAL RRS LINE INTENSITIES.

EXPERIMENT NO.	=091572B
GAS	=02
WAVELENGTH IN NM	=647.1
POLARIZATION	=UR
TEMP. IN C	=75
PRESSURE IN TORR	=732.0
POWER IN WATTS	=.320
U-VALUE*10**47	=15.95
NORM. CONST.	= 44.8

J	EXPERIMENTAL LINE INTENSITY	THEORETICAL LINE INTENSITY	THEORETICAL % STAND. DEV.	RATIO: DEV. TO STAND.DEV.
STOKES				
1	56.80	75.56	5.14	-4.82
3	122.40	131.21	3.90	-1.72
5	167.60	170.59	3.42	-0.51
7	191.60	190.70	3.24	0.15
9	198.20	191.79	3.23	1.04
11	174.00	177.16	3.36	-0.53
13	153.40	152.01	3.63	0.25
15	111.20	122.00	4.05	-2.19
17	98.60	91.98	4.66	1.54
19	68.00	65.36	5.53	0.73
21	39.00	43.86	6.75	-1.64
23	27.00	27.84	8.48	-0.36
25	13.40	16.74	10.93	-1.83
27	8.60	9.55	14.47	-0.68
ANTISTOKES				
3	51.00	72.06	5.27	-5.55
5	120.20	120.48	4.07	-0.06
7	152.00	150.81	3.64	0.22
9	165.00	162.31	3.51	0.47
11	165.80	157.15	3.57	1.54
13	140.80	139.76	3.78	0.20
15	115.00	115.46	4.16	-0.10
17	85.00	89.21	4.73	-1.00
19	66.60	64.76	5.56	0.51
21	45.80	44.30	6.72	0.50
23	27.00	28.62	8.36	-0.68
25	19.20	17.49	10.69	0.91
27	9.00	10.13	14.05	-0.79

TABLE 22. COMPARISON OF THEORETICAL AND EXPERIMENTAL RRS LINE INTENSITIES.

EXPERIMENT NO.	=091972A
GAS	=N2
WAVELENGTH IN NM	=647.1
POLARIZATION	=UR
TEMP. IN C	=125
PRESSURE IN TORR	=736.8
POWER IN WATTS	=.302
U-VALUE*10**47	=6.36
NORM. CONST.	= 47.6

J	EXPERIMENTAL LINE INTENSITY	THEORETICAL LINE INTENSITY	THEORETICAL % STAND. DEV.	RATIO: DEV. TO STAND.DEV.
STOKES				
0	10.60	12.15	12.83	-0.99
1	6.20	10.74	13.65	-3.10
2	24.80	29.71	8.20	-2.01
3	16.20	18.38	10.43	-1.14
4	39.60	42.43	6.87	-0.97
5	23.00	23.30	9.26	-0.14
6	50.40	49.21	6.37	0.38
7	27.40	25.14	8.92	1.01
8	50.40	49.93	6.33	0.15
9	28.00	24.16	9.10	1.75
10	51.80	45.66	6.62	2.03
11	20.60	21.10	9.74	-0.24
12	41.00	38.20	7.24	1.01
13	15.20	16.94	10.86	-0.95
14	30.40	29.49	8.23	0.37
15	10.80	12.60	12.60	-1.13
16	23.60	21.13	9.73	1.20
17	10.20	8.71	15.16	1.13
18	10.40	14.10	11.91	-2.20
19	8.00	5.61	18.87	2.25
20	9.80	8.79	15.08	0.76
ANTISTOKES				
2	12.00	11.75	13.05	0.16
3	8.00	10.16	14.03	-1.51
4	25.60	27.49	8.53	-0.80
5	16.20	16.63	10.97	-0.23
6	34.80	37.55	7.30	-1.00
7	19.40	20.17	9.96	-0.38
8	37.80	41.65	6.93	-1.33
9	19.60	20.81	9.80	-0.59
10	40.00	40.42	7.03	-0.15
11	18.20	19.13	10.23	-0.47
12	32.80	35.35	7.52	-0.96
13	16.60	15.98	11.19	0.35
14	33.20	28.29	8.41	2.06
15	12.80	12.27	12.77	0.34
16	22.80	20.89	9.78	0.93
17	7.60	8.73	15.14	-0.85
18	13.60	14.32	11.82	-0.43
19	5.80	5.77	18.62	0.03
20	10.40	9.14	14.79	0.93

TABLE 23. CØMPARISØN ØF THEØRETICAL AND EXPERIMENTAL RRS LINE INTENSITIES.

EXPERIMENT NØ.	=091972B
GAS	=N2
WAVELENGTH IN NM	=647.1
PØLARIZATIØN	=R
TEMP. IN C	=125
PRESSURE IN TØRR	=736.8
PØWER IN WATTS	=.297
U-VALUE*10**47	=6.36
NØRM. CØNST.	= 50.3

J	EXPERIMENTAL LINE INTENSITY	THEØRETICAL LINE INTENSITY	THEØRETICAL % STAND. DEV.	RATIØ: DEV. TØ STAND.DEV.
STØKES				
0	7.60	10.16	14.03	-1.80
1	4.20	8.98	14.92	-3.57
2	21.80	24.85	8.97	-1.37
3	15.00	15.37	11.41	-0.21
4	36.60	35.48	7.51	0.42
5	17.60	19.48	10.13	-0.95
6	41.60	41.14	6.97	0.16
7	19.60	21.01	9.76	-0.69
8	42.80	41.73	6.92	0.37
9	21.40	20.19	9.95	0.60
10	38.40	38.15	7.24	0.09
11	14.40	17.63	10.65	-1.72
12	28.40	31.90	7.92	-1.39
13	10.40	14.15	11.89	-2.23
14	21.60	24.63	9.01	-1.36
15	13.40	10.52	13.79	1.99
16	20.00	17.64	10.65	1.26
17	7.80	7.27	16.59	0.44
18	13.20	11.77	13.04	0.93
19	6.80	4.68	20.66	2.19
20	6.80	7.33	16.51	-0.44
ANTIST3KES				
2	6.40	9.83	14.26	-2.45
3	4.60	8.50	15.34	-2.99
4	23.60	23.01	9.32	0.28
5	14.60	13.92	11.99	0.41
6	32.00	31.44	7.98	0.22
7	19.20	16.89	10.88	1.26
8	31.00	34.89	7.57	-1.47
9	21.80	17.43	10.71	2.34
10	39.20	33.86	7.69	2.05
11	17.20	16.03	11.17	0.66
12	29.20	29.63	8.22	-0.17
13	15.40	13.39	12.22	1.23
14	20.40	23.71	9.18	-1.32
15	15.40	10.29	13.94	3.56
16	15.80	17.52	10.69	-0.92
17	8.20	7.32	16.53	0.73
18	14.40	12.01	12.91	1.54
19	4.20	4.84	20.33	-0.65
20	7.00	7.67	16.15	-0.54

TABLE 24. CØMPARISØN ØF THEØRETICAL AND EXPERIMENTAL RRS LINE INTENSITIES.

EXPERIMENT NØ.	=091972D
GAS	=Ø2
WAVELENGTH IN NM	=647.1
PØLARIZATIØN	=UR
TEMP. IN C	=124
PRESSURE IN TØRR	=730.4
PØWER IN WATTS	=.302
U-VALUE*10**47	=15.95
NØRM. CØNST.	= 48.1

J	EXPERIMENTAL LINE INTENSITY	THEØRETICAL LINE INTENSITY	THEØRETICAL % STAND. DEV.	RATIØ: DEV. TØ STAND.DEV.
STØKES				
1	40.20	58.59	5.84	-5.37
3	91.00	102.51	4.42	-2.54
5	134.80	135.08	3.85	-0.05
7	147.40	153.96	3.60	-1.18
9	153.80	158.82	3.55	-0.89
11	152.80	151.37	3.63	0.26
13	138.00	134.83	3.85	0.61
15	110.60	112.99	4.21	-0.50
17	90.00	89.50	4.73	0.12
19	70.80	67.20	5.46	0.98
21	52.00	47.94	6.46	1.31
23	28.80	32.55	7.84	-1.47
25	29.40	21.06	9.74	4.06
27	15.40	13.00	12.41	1.49
ANTISTØKES				
3	45.80	56.29	5.96	-3.13
5	87.40	95.40	4.58	-1.83
7	117.20	121.75	4.05	-0.92
9	147.60	134.40	3.86	2.55
11	128.40	134.28	3.86	-1.13
13	128.40	123.96	4.02	0.89
15	112.00	106.94	4.32	1.09
17	86.20	86.80	4.80	-0.14
19	74.00	66.59	5.48	2.03
21	50.20	48.43	6.43	0.57
23	37.00	33.46	7.73	1.37
25	23.20	22.01	9.53	0.57
27	16.60	13.79	12.04	1.69

TABLE 25. COMPARISON OF THEORETICAL AND EXPERIMENTAL RRS LINE INTENSITIES.

EXPERIMENT NO.	=091972C
GAS	=02
WAVELENGTH IN NM	=647.1
POLARIZATION	=R
TEMP. IN C	=125
PRESSURE IN TORR	=730.4
POWER IN WATTS	=.297
U-VALUE*10**47	=15.95
NORM. CONST.	= 46.3

J	EXPERIMENTAL LINE INTENSITY	THEORETICAL LINE INTENSITY	THEORETICAL % STAND. DEV.	RATIO: DEV. TO STAND.DEV.
STOKES				
1	33.00	44.67	6.69	-3.90
3	77.20	78.14	5.06	-0.24
5	101.80	102.95	4.41	-0.25
7	112.00	117.32	4.13	-1.10
9	120.60	120.99	4.07	-0.08
11	118.40	115.30	4.16	0.65
13	103.40	102.68	4.41	0.16
15	87.00	86.03	4.82	0.23
17	68.60	68.13	5.42	0.13
19	55.40	51.15	6.25	1.33
21	39.60	36.48	7.40	1.15
23	26.00	24.77	8.99	0.55
25	17.60	16.02	11.17	0.88
27	9.00	9.88	14.22	-0.63
ANTISTOKES				
3	34.40	42.94	6.82	-2.91
5	67.80	72.78	5.24	-1.31
7	91.20	92.90	4.64	-0.40
9	102.40	102.58	4.42	-0.04
11	104.00	102.50	4.42	0.33
13	98.60	94.64	4.60	0.91
15	81.00	81.66	4.95	-0.16
17	66.40	66.30	5.49	0.03
19	56.40	50.87	6.27	1.73
21	35.40	37.00	7.35	-0.59
23	28.40	25.57	8.84	1.25
25	18.00	16.82	10.90	0.64
27	10.60	10.54	13.77	0.04

height analyzer began to behave erratically, and was replaced with a standby unit. Although attempts were made to return the system to the same sensitivity, this change probably left some remnant shift. Such a shift may account for the consistently smaller normalization constants obtained for the experiments at 647.1 nm. Furthermore, although no long term studies of the stability of RCA C31000D photomultipliers are available, our experience with other high quality photomultipliers includes substantial shifts in sensitivity.

With respect to the second point, the entrance slit widths used in the spectra measurements were narrower than the image of the incident beam. In this situation the signal strength is extremely sensitive to small changes in alignment. Furthermore, the lasers used in these experiments can operate in several transverse modes and they shift mode occasionally. Such a shift will change the beam profile and, if narrow slits are used, a significant change in sensitivity can result thereby.

To summarize these comments, when narrow slits are used or comparisons made of results taken several days apart, we have observed signal variations greater than 10% in spite of efforts to minimize such variations. For this reason we use wide slits and frequent calibrations in cross section measurements. Likewise, the variations in normalization constant are likely to be the result of changes in overall system sensitivity, rather than indications of a true departure between experiment and theory. This expectation is supported by auziliary experiments in which we observed the variation of single line intensities in N_2 and O_2 as temperature was increased from 23°C to 125°C. The results are shown in Table 26. Within an experimental accuracy of about ±5%, these line intensities followed the temperature dependence predicted by Eq. 64.

Within the individual spectra, the simple statistical analysis we have undertaken reveals no inconsistency between experimental and theoretical results, with one possible exception. In the RRS spectra for N_2 with incident light at 488.0 nm in the UR polarization state (Experiments 090172C, 090672B, and 090772A) the first Stokes and anti-Stokes lines (J=0 and 2, respectively) are too large by factors between 2 and 3. These lines are on the edge of the high background surrounding the Rayleigh scattering. Subsequently we have evaluated the background by observing laser light scattered from the reference screen. This evaluation leads to the conclusion that these high counts probably are due to background, but a slight possibility remains that the discrepancy is significant.

Table 26. Temperature dependence of RRS lines of N_2 and O_2. The incident light wavelength is 647.1 nm and the slit settings are 250/500/250 μm. These results are distinguished by relatively wide slit settings and the fact that they were obtained over a relatively short time period (four hours) to minimize the effects of any drift in system response. The relative theoretical count rate r_T is calculated from $r_T = (F\sigma)\,\Theta_o p\,/(F\sigma)_o \Theta p_o$, where Θ and p denote g as temperature and pressure, respectively, and the subscript "o" indicates values at the lowest temperature. The symbol r_x indicates experimental count rate ratios and the error estimate is the theoretical standard deviation of the count rate, averaged over counting periods.

Transition	Θ (^oK)	p (torr)	C (count/sec)	r_x	r_t
N_2:J= 6→8	296	700	184	1.000	1.000
	358	711	139	.755±.035	.745
	433	722	104	.567±.030	.548
O_2:N= 9→11	305	711	302	1.000	1.000
	438	722	104	.585±.018	.589

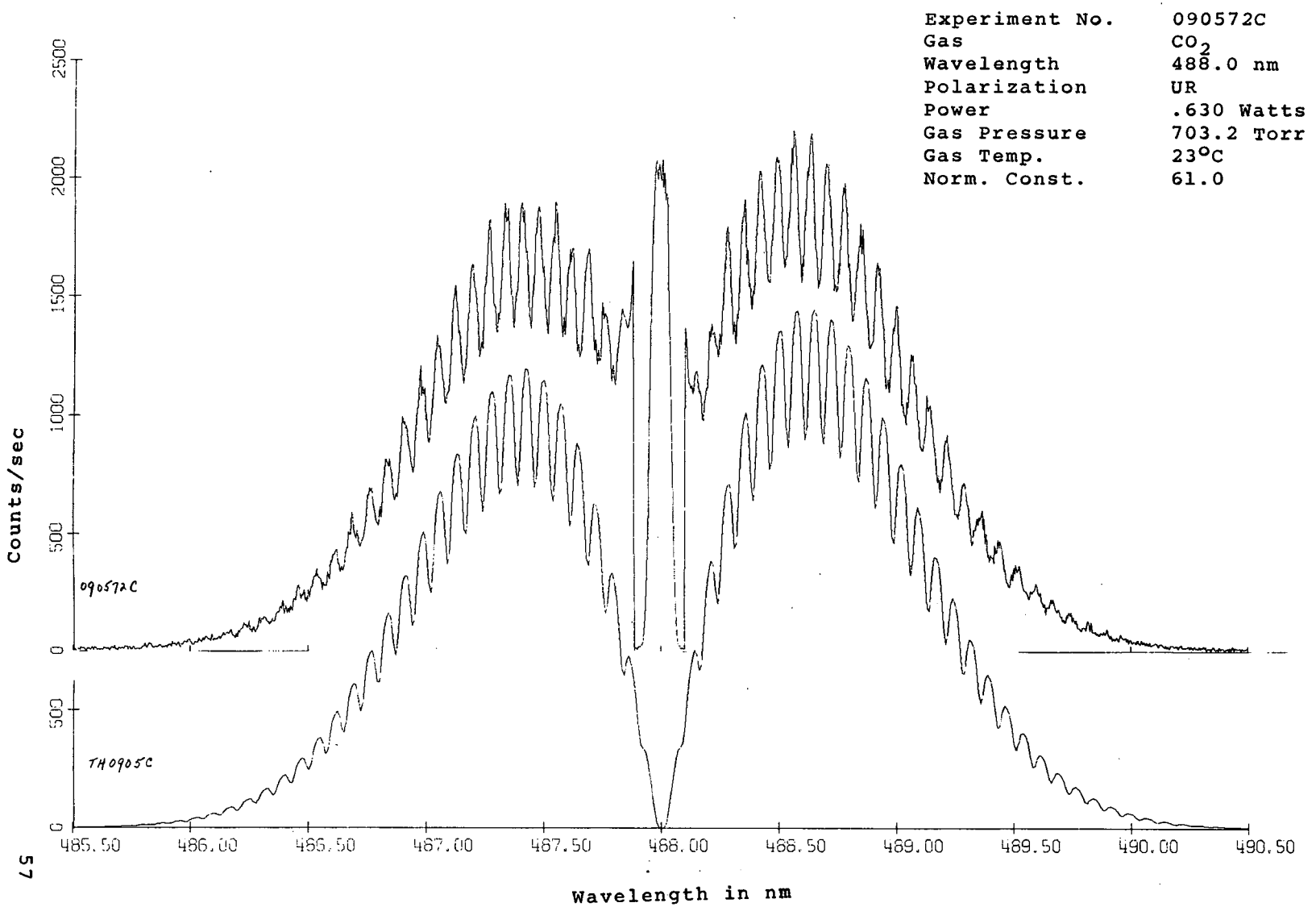

Figure 5. Comparison of experimental and theoretical rotational Raman spectra of CO_2.

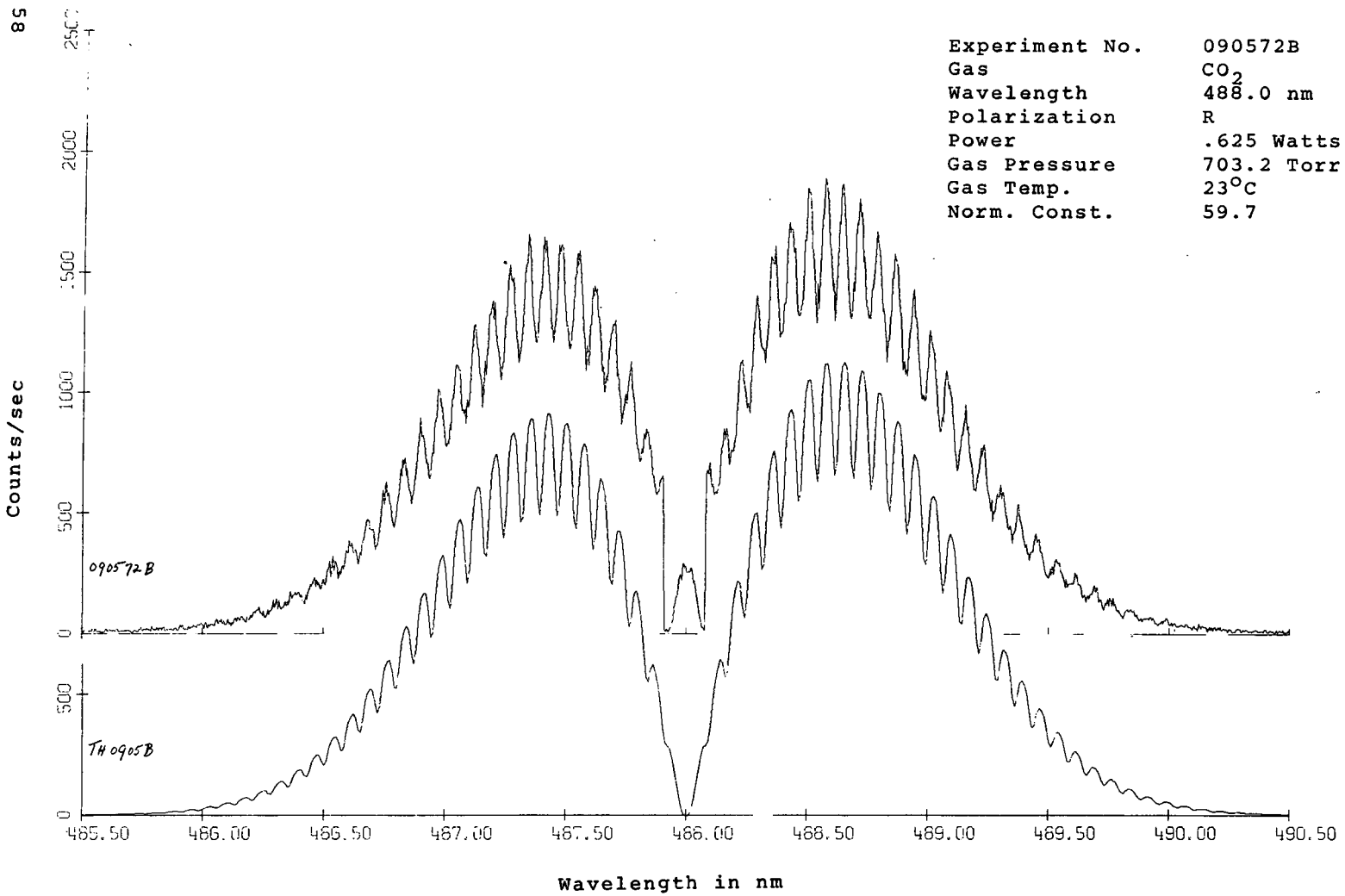

Figure 6. Comparison of experimental and theoretical rotational Raman spectra of CO_2.

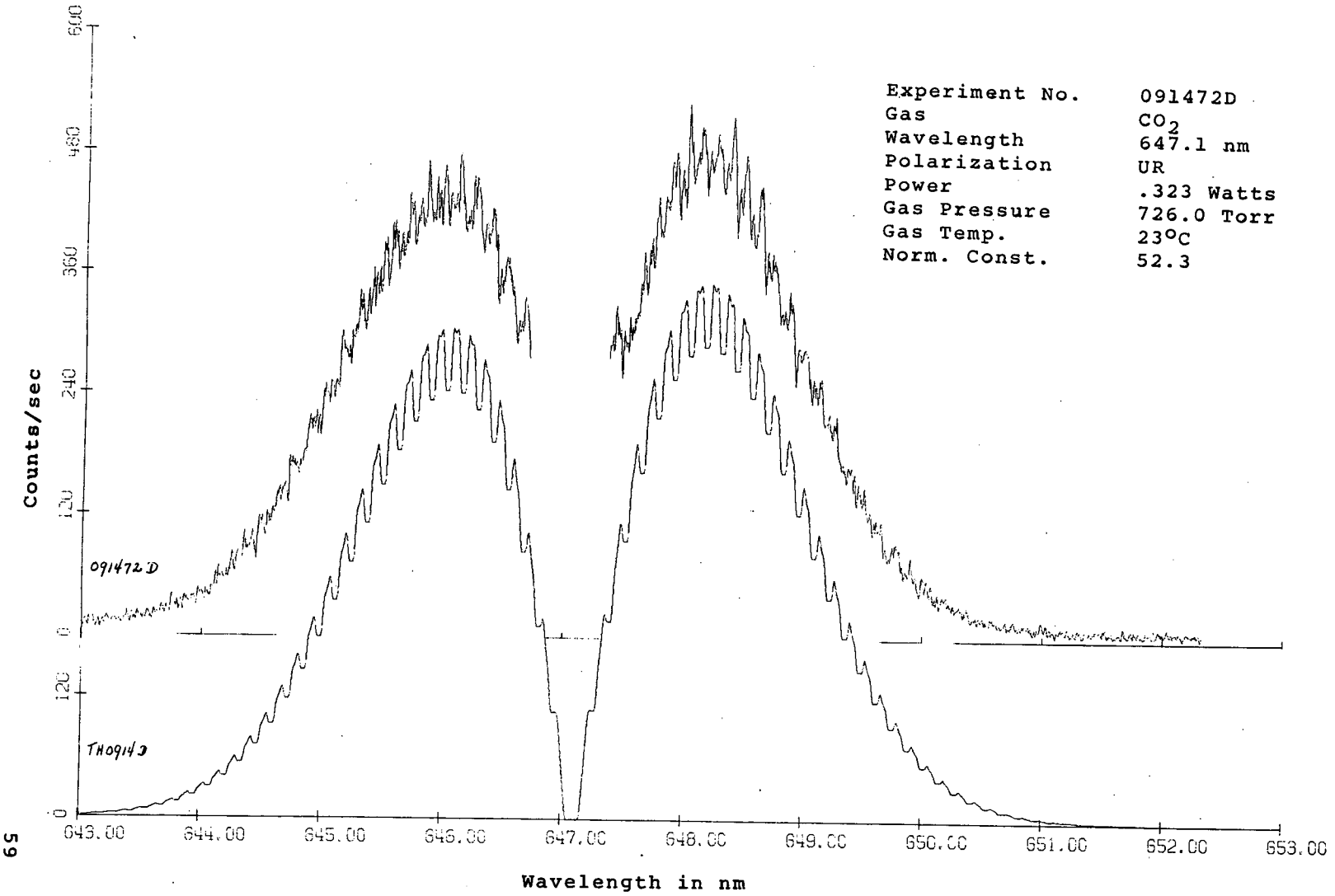

Figure 7. Comparison of experimental and theoretical rotational Raman spectra of CO_2.

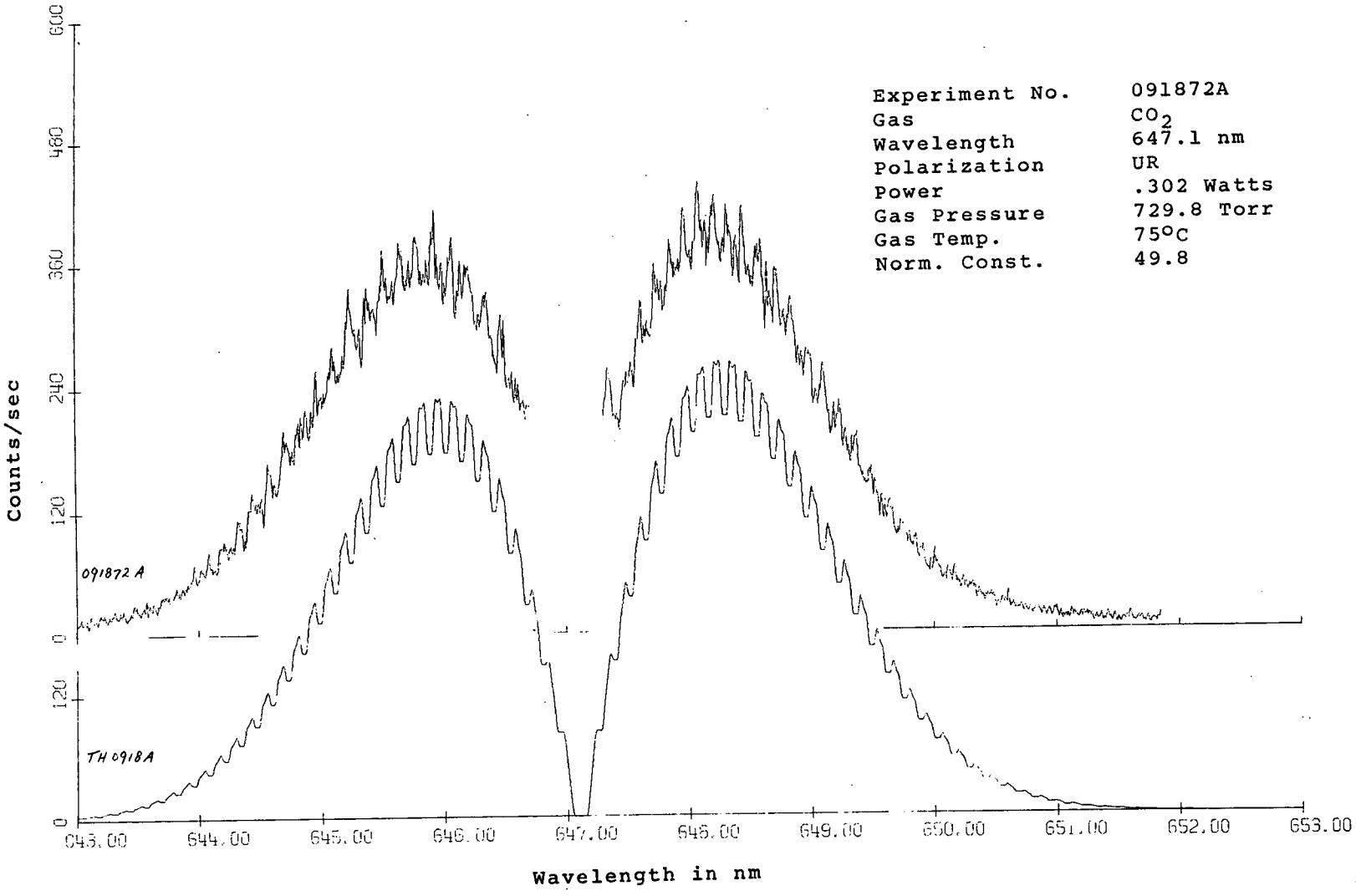

Figure 8. Comparison of experimental and theoretical rotational Raman spectra of CO_2.

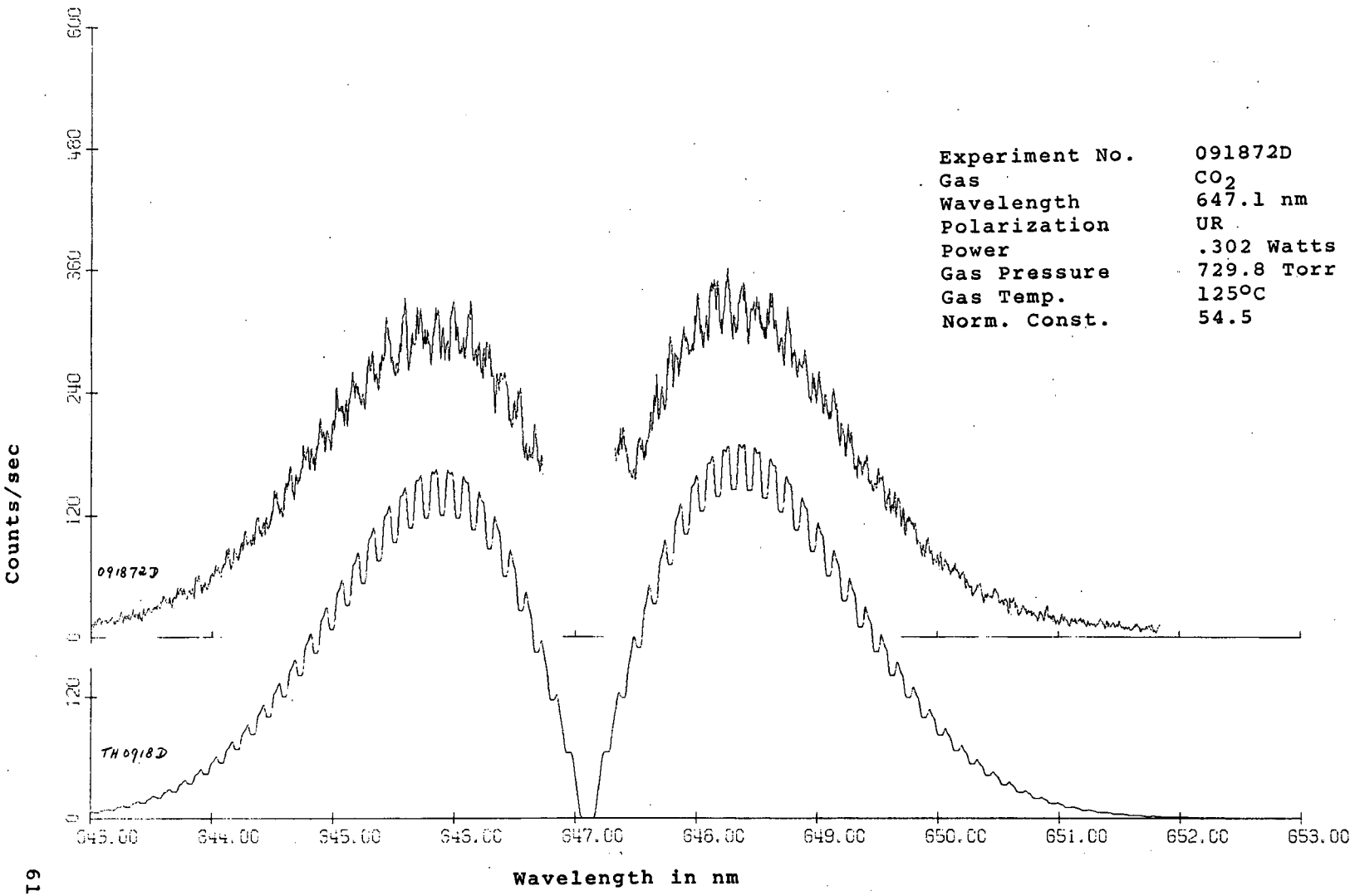

Figure 9. Comparison of experimental and theoretical rotational Raman spectra of CO_2.

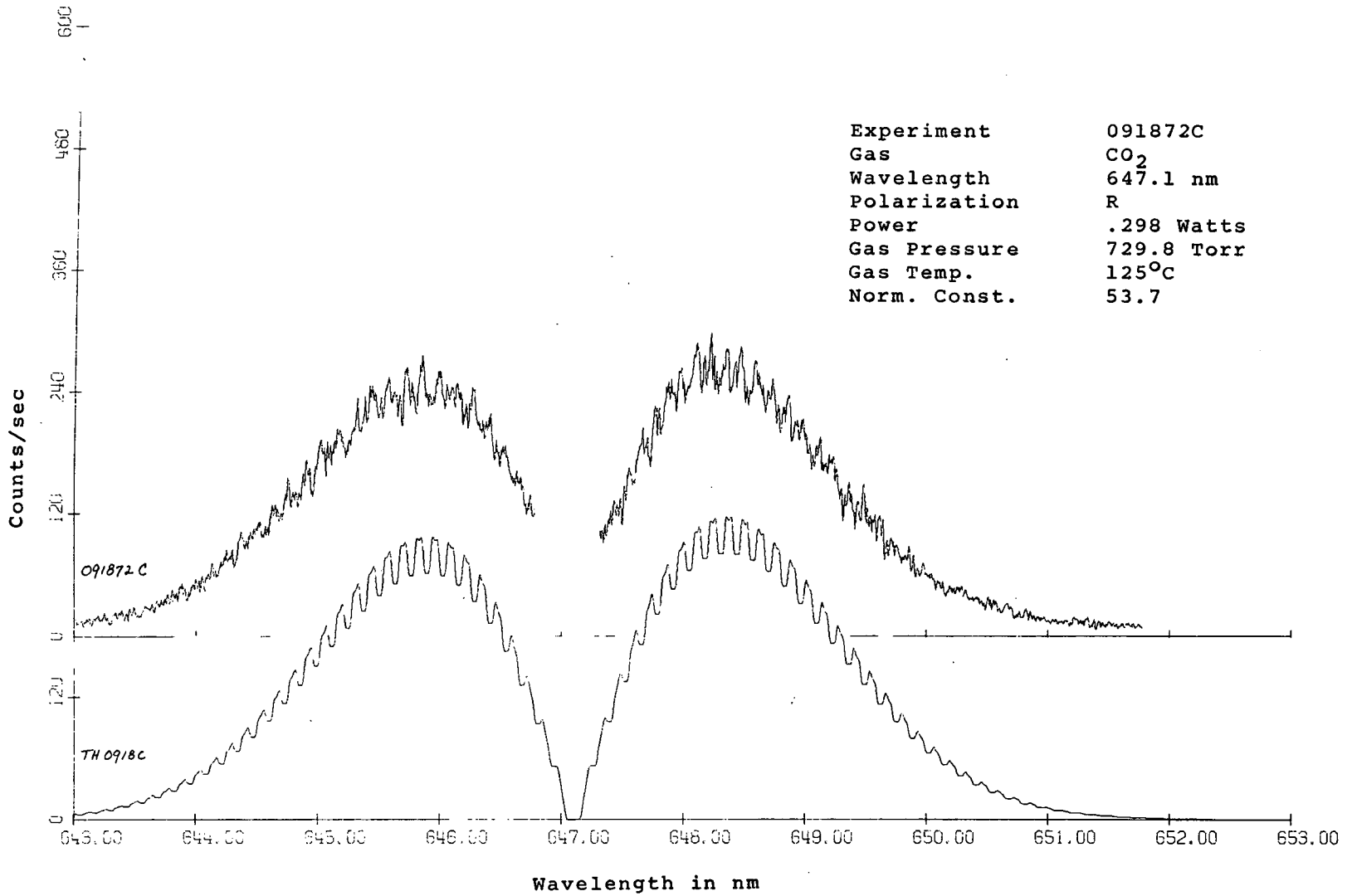

Figure 10. Comparison of experimental and theoretical rotational Raman spectra of CO_2.

Carbon Dioxide

Experimental spectra for CO_2 are shown in Figs. 5 through 10. Corresponding theoretical spectra are also shown on these figures for comparison. The theoretical spectra were generated using Eq. 64 with measured slit functions. Eq. 64 is strictly correct only for SLM. Since the RRS spectra of CO_2 departs slightly from that of a SLM at room temperature, and more at higher temperatures, the experimental and theoretical spectra shown in the figures should not be expected to be in optimum quantitative agreement. However, the qualitative agreement is quite good.

CONCLUSIONS

Reasonable agreement exists between our measurements of absolute intensity factors (U-values) for rotational Raman scattering (RRS) and calculation of these factors from recent measurements of the depolarization of Rayleigh scattering plus RRS. This agreement supports a conclusion that the absolute intensity of RRS from N_2, O_2 and CO_2 can be calculated to useful accuracy (estimated errors ranging from 8 to 15%) from the results presented herein.

Measurements of the depolarization at 488.0 nm average about 3% lower than the theoretical value of 3/4 whereas the average of those at 647.1 nm is 0.750. Additional experiments would be needed to evaluate the significance of the small discrepancy at 488.0 nm. Nevertheless, these results support a conclusion that the depolarization of strong RRS lines of N_2, O_2 and CO_2 is at least within a few percent of the theoretical value under the stated experimental conditions.

Our measurements of the relative intensities of lines within RRS spectra (Tables 10-25) allow this conclusion to be extended to all observed lines with reduced but still useful precision. The observed deviations in line intensities from theoretical predictions within individual spectra are somewhat larger than predicted from signal statistics. It is likely that the excess fluctuations are due primarily to drifts in system sensitivity. Experience leads us to believe that such drifts are a price usually paid for use of narrow slits. Nevertheless, useful precision is retained, providing a substantial verification of the theoretical description of relative RRS line intensities within individual spectra.

On the other hand, fluctuations in the normalization constants for separate spectra are too large to confirm theoretical predictions for the temperature dependence of individual lines. Therefore, in an auxiliary experiment the intensities of several lines of N_2 and O_2 were monitored as a function of temperature using wide slits. The results (Table 26) follow the theoretical

predictions very closely. Furthermore they serve to link the individual narrow slit spectra, providing further indication that RRS is described accurately by the theoretical predictions. The only notable exceptions are the anomalously large signals attributed to first Stokes and anti-Stokes lines of N_2 excited by 488.0 nm radiation in the UR polarization state. This discrepancy may arise from a low background estimate.

APPENDIX A. ANGLE DEPENDENCE OF CROSS SECTION

The angle dependence of Rayleigh and Raman cross sections is given by Eq. 2 in the text, which is reproduced below:

$$\sigma = \sigma_{zz}[(1-\rho)\cos^2\psi+\rho]$$

Here ψ is the angle between polarization of incident and scattered light. Frequently, it is useful to express $\cos^2\psi$ in terms of other scattering angles. One set of such angles, which is useful if the incident light is linearly polarized or unpolarized, is shown in Fig.11.

As an example of the use of this set of angles, we consider the cross section for the scattering summed over polarization states. Convenient states are those for which ξ=0 and 90°. The resulting cross section is

$$\sigma(\theta,\phi) = \sigma_{zz}[(1+\rho)-(1-\rho)\sin^2\theta\cos^2\phi] \qquad \text{(A1)}$$

Integration of this result over all angles yields for the total cross section

$$\sigma^T = \frac{8\pi}{3}\sigma_{zz}(1+2\rho) \qquad \text{(A2)}$$

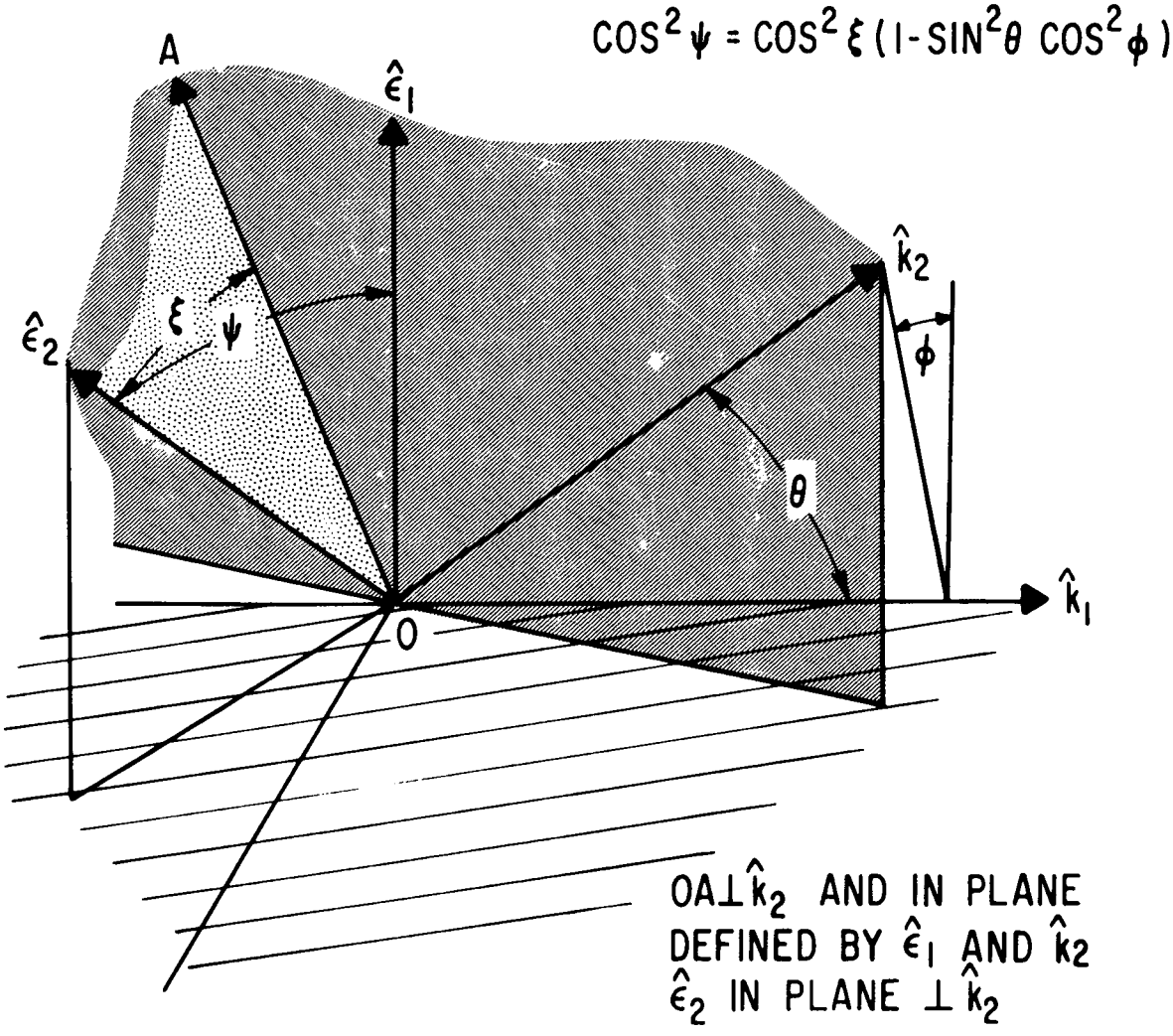

Figure 11. Coordinate system for analysis of angular dependence of scattering. The unit vectors $\hat{k}_1$, $\hat{\epsilon}_1$, $\hat{k}_2$ and $\hat{\epsilon}_2$ define the directions of propagation and polarization of incident and scattered light, respectively.

APPENDIX B. DETAILS OF ROTATIONAL RAMAN SPECTRA OF CARBON DIOXIDE AND OXYGEN

Carbon Dioxide

In its ground electronic and vibrational state, CO_2 is a simple linear molecule (SLM) i.e. it is linear with no electronic angular momentum. However, even at room temperature the first excited vibrational state of CO_2 is significantly populated ($\sim$8%). Since this state is not totally symmetric, the RRS from molecules in it is more complicated than that from the SLM. An excellent analysis of the resulting RRS spectra has been presented by Barrett and Weber (ref.12). It is evident from their work that at room temperature the contribution from the excited state is not large. Thus our analysis in terms of a SLM is a reasonable approximation. However, in the main body of this paper we have included information about slit settings, and spectrometer dispersion in order to facilitate a more detailed analysis.

Oxygen

The O_2 rotational Raman spectrum (ref 11, 20, 21, 22, 23) is more complicated than that for N_2 because the ground electronic state of O_2 is a triplet (i.e., the spin quantum number S = 1), whereas the ground electronic state of N_2 is a singlet (i.e., S = 0). For triplet states, three rotational sublevels correspond to each rotational level of an "equivalent" singlet molecule. (See Fig.12.) Here, the quantum number N, corresponding to <u>total</u> angular momentum J minus spin S, is introduced.

Because of the additional structure to the energy levels, more types of transitions are possible for triplet systems than for singlets. Thus, for the $\Delta N = 0, \pm 2$ transitions of the rotational Raman spectrum, transitions exist for $J = 0, \pm 1, \pm 2$. This gives rise to two additional "satellite" components adjacent to each of the Raman lines as shown in Fig.13. These satellite" components fall off in intensity rapidly with increasing values of N, since the line strengths (i.e., purely N-dependent factors in th- intensity relations) of the corresponging transitions vary as $1/N$ and $1/N^3$, while the line strengths of the "main" components vary as N.

For present purposes it is essential to know accurately the total intensities and, in particular, to know whether or not they differ from those predicted by the Placzek-Teller coefficients (ref.24).

In order to consider this situation in detail, we study the Stokes band, for which $\Delta N = +2$. Here, ΔJ can be 0, +1, or +2. Use of the relations from Renschler et al (ref.11) for rotational line strength $S(J,N|J',N')$, corresponding to the transition

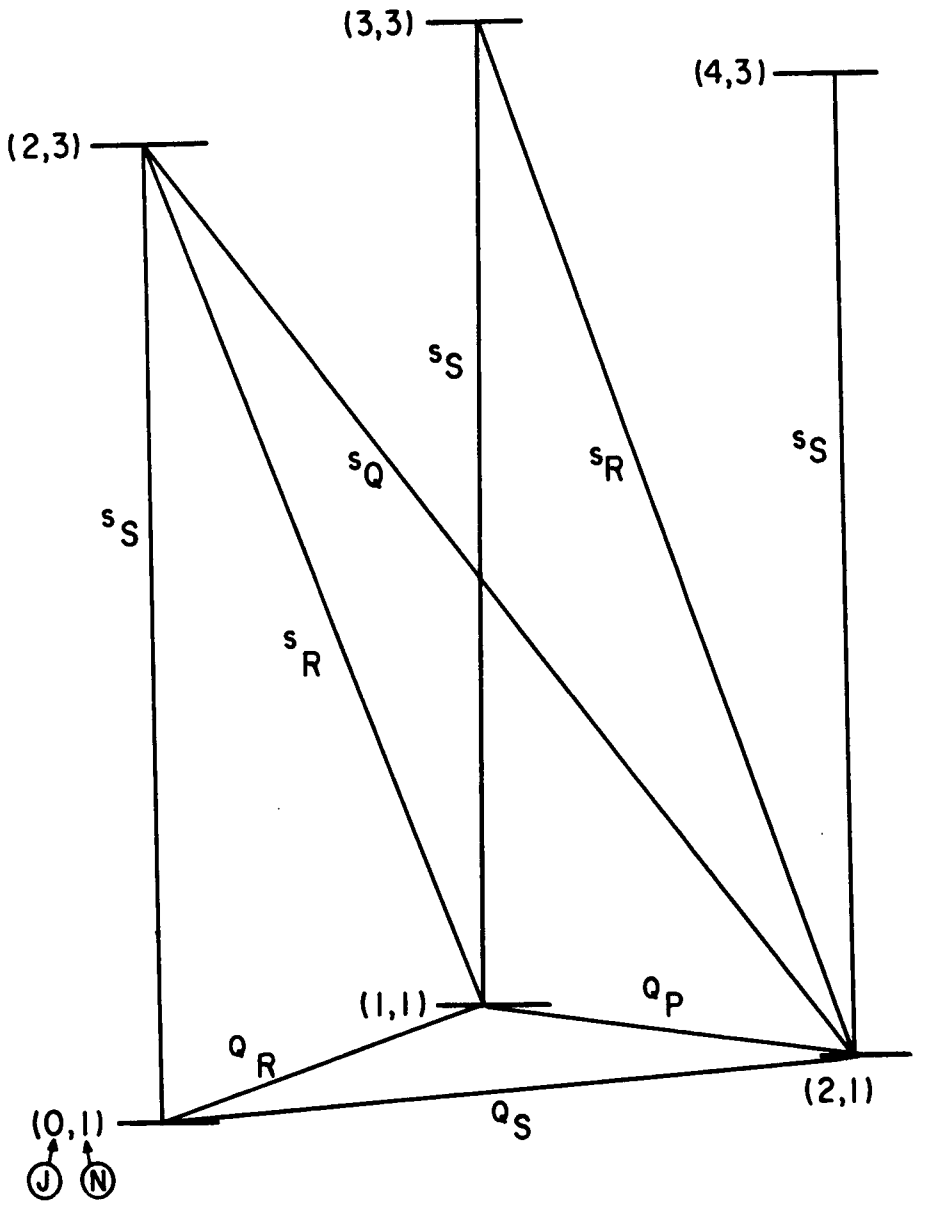

Figure 12. Lowest energy levels of the Oxygen molecule ($3\Sigma_g^-$ electronic ground state).

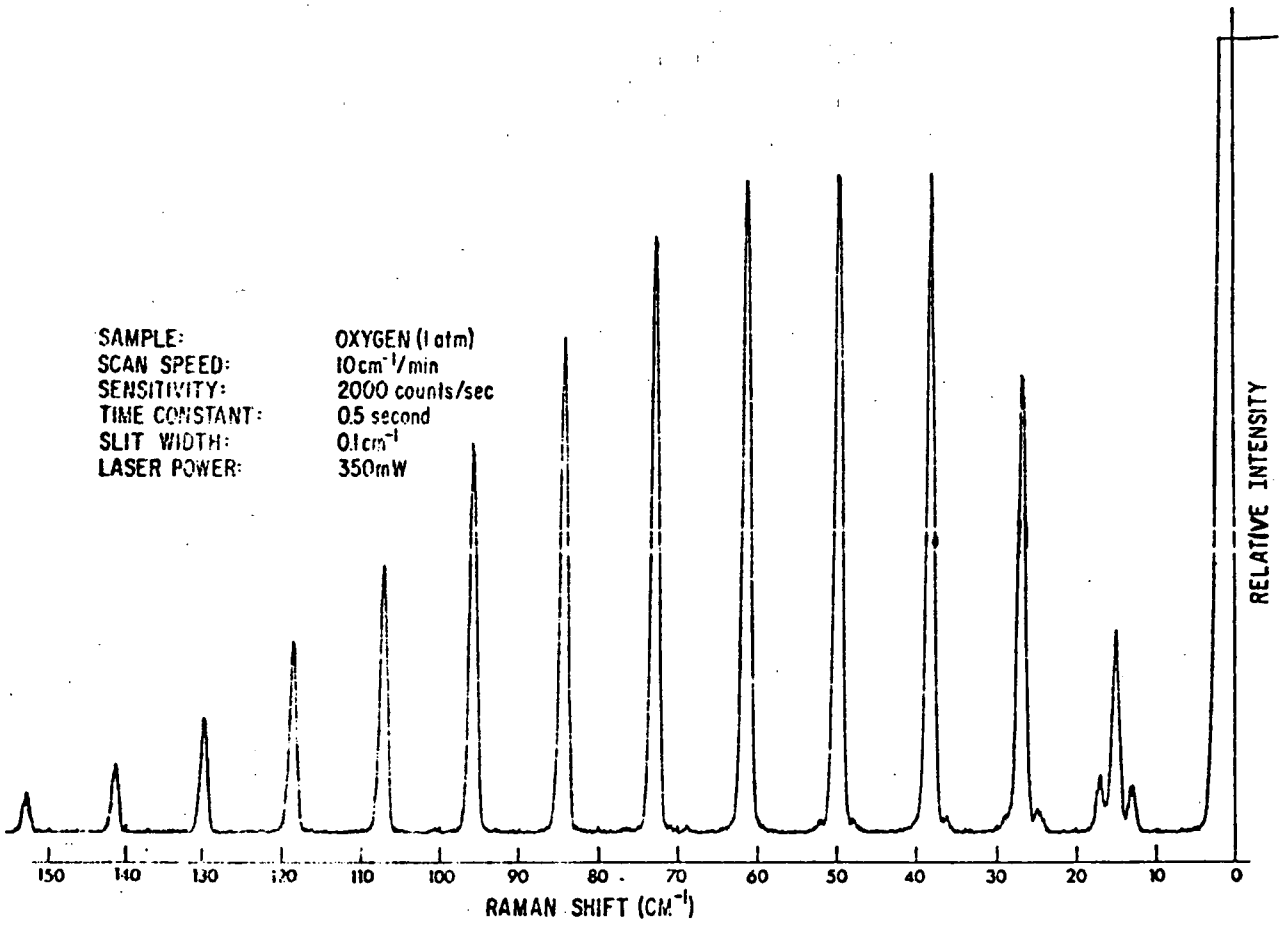

Figure 13. High resolution experimental trace of rotational Raman scattering from O_2, taken by Dr. James N. Willis, Jarell-Ash Division, Fisher Scientific Co.

J,N→J',N', leads to the conclusion that the sum of these line strengths is the same as is obtained by simply ignoring the spin; that is

$$\sum_{J,J'} b(J,N:J',N+2) = 3(2N+1)b^{N}_{N+2} \ .$$

Here the factor 3 arises because each value of the quantum number N corresponds to three values of J with J equal to N, N+1, or N-1. The factors b^{N}_{N+2} are a specialization of a Placzek-Teller coefficient (which is, in its general form, valid for the more complicated situation of a symmetric top molecule.) For this case,

$$b^{N}_{N+2} = \frac{3}{2} \frac{(N+1)(N+2)}{(2N+1)(2N+3)}$$

Thus we are justified in treating oxygen as a simple linear molecule insofar as the "total" RRS line strengths (main line plus satellites) are concerned. The slit functions used in the O_2 cross section measurements were sufficiently wide to observe this total line strength. In fact the only results of this work which should be affected by the spin structure are the low N lines of the O_2 RRS spectra measurements. Since the spin satellites are weak, even this effect will be small.

APPENDIX C. ERROR ESTIMATES

Several types of errors can contribute to the total expected error in cross section and depolarization measurements. The detector pulse counts involved in all of these measurements have statistical variations described to good approximation by a Poisson distribution. Furthermore, both relative and absolute calibrations of detectors and reference lamps can be expected to be somewhat in error. The sensitivity of photomultiplier detectors can vary a few percent over a period of an hour, and vibration and temperature changes can alter the alignment of a monochromator. Our system and experimental techniques have been chosen to minimize such system variations. Nevertheless, we have observed variations in system response of 2% in one hour, and occasionally 8% over a day. Accordingly, we expect measurements completed in short time periods, such as those of relative O_2/N_2 cross sections and depolarization, to be more accurate than measurements requiring a longer time.

In the following calculations of error estimates, contributions from the statistical fluctuations in count rate are expressed in terms of standard deviation. Uncertainties in the calibration of the incident beam power monitor and the reference lamp (including the reference diffusing screen) are expressed in terms of probable errors derived from manufacturer's statements and our own experiences with comparable calibrations. No attempt is made to evaluate remnant systematic errors. In most cases where there is a strong theoretical expectation of a particular result, (such as is the case for depolarization or Rayleigh cross section) the deviation between experimental and theoretical results is within the estimated error computed as described above.

Expressions for the cross sections and depolarization in terms of experimental values take the form of functions of these values; i.e.

$$A = f(X_1, X_2, X_3, X_4 \ldots) \tag{C1}$$

In such cases, the expected error ΔA can be computed approximately using the method of propagation of errors. This approximation is accurate if the individual relative errors, such as $\Delta X_1/X_1$, are much less than 1, and if the resulting relative changes in A are also small; i.e. if

$$\frac{1}{A}\ \frac{df}{dX_1}\ \Delta X_1 \ll 1. \tag{C2}$$

These conditions are satisfied in the present case. Then the expected error in A is given by

$$\Delta A \simeq \left[\sum_j \left(\frac{df}{dx_j}\right)^2 (\Delta x_j)^2 \right]^{1/2} \qquad \text{(C3)}$$

In particular, the cross section and depolarization expression can be put in the general form of products and/or quotients; i.e.

$$A = \frac{B \cdot C \cdots}{D \cdot E \cdots} \qquad \text{(C4)}$$

Then using Eq.C3 it can be shown readily that the relative expected error in A is given by

$$\frac{\Delta A}{A} \simeq \left[\left(\frac{\Delta B}{B}\right)^2 + \left(\frac{\Delta C}{C}\right)^2 + \cdots + \left(\frac{\Delta D}{D}\right)^2 + \left(\frac{\Delta E}{E}\right)^2 + \cdots \right]^{1/2} \qquad \text{(C5)}$$

On the other hand, the net photomultiplier count C_N used in a measurement is obtained as the average of a series of gross counts C_G minus a background count b which we shall assume is known. Thus

$$C_N = \frac{1}{n} \sum_{j=1}^{n} (C_G)_j - b = \langle C_G \rangle - b \qquad \text{(C6)}$$

If the statistical fluctuations in C_G are Poisson - distributed, then the relative S.D. in C_N is given by

$$\frac{\Delta C_N}{C_N} = \frac{1}{C_N} \left(\frac{1}{n} \langle C_G \rangle\right)^{1/2} \qquad \text{(C7)}$$

These general results will be used in the determination of estimated errors which follow.

Error Estimates for Absolute Measurements

The calculation of cross sections from separate absolute measurements of incident beam and scattered light power are accomplished using Eq. 45. Here the predominant contributions to the expected error are those in the measurement of incident beam power P, reference lamp irradiance I_λ, and scattering count rate C. Based on manufacturer's statements and our own

experience, we estimate the following relative errors for P and I_λ measurements:

$$\frac{\Delta P}{P} = 10\%$$

$$\frac{\Delta(I_\lambda)}{I_\lambda} = 15\%$$

A typical result for the relative S.D. in the count rate is obtained for the N_2 J= 8→10 line at 6471Å (Table 4, Exp. #4). In this measurement, C_o^s = 26.7 counts per one second interval, as determined by an average over 25 intervals. The background for this measurement was 7 counts/sec. Thus

$$\frac{\Delta C_o^s}{C_o^s} = \frac{1}{26.7}\left[\frac{1}{25}\quad 33.7\right]^{1/2} \qquad (C8)$$

$$= 4.4\%$$

Combining these contributions in accordance with Eq. C5, we obtain the following result for the estimated relative error in this example absolute measurement:

$$\frac{\Delta(F\sigma)_A}{(F\sigma)_A} = \left[(15\%)^2 + (10\%)^2 + (4.4\%)^2\right]^{1/2} \simeq 18\% \qquad (C9)$$

The estimated errors for the other absolute measurements in Table 4 are also approximately ±18%, because the only factor which changes substantially between measurements is the count rate, and its influence on the estimated error is small.

Error Estimates for Nitrogen Cross Section from Raman/Rayleigh Ratios

The Raman/Rayleigh ratio Z is calculated in effect from the following expression

$$Z = \frac{(C_o^s)_{RAM}}{(C_o^s)_{RAY}} \quad \frac{I_{\lambda RAY}}{I_{\lambda RAM}} \quad \frac{(C_o)_{RAY}}{(C_o)_{RAM}} \quad \frac{(\frac{1+\alpha}{1+\rho\alpha})_{RAM}}{(\frac{1+\alpha}{1+\rho\alpha})_{RAY}} \qquad (C10)$$

In our experiments the relative S.D. in $(C_o^s)_{RAM}$ is between 4 and 5%. We estimate the relative error in the ratio $(I_{\lambda RAY}/I_{\lambda RAM})$ to be 5%, based on observed fluctuations in lamp intensity. The quantities $(C_o^s)_{RAY}$, $(C_o)_{RAY}$ and $(C_o)_{RAM}$ have S.D. on the order of 1%. In these calculations ρ_{RAM} is assumed to be 75% and $\rho_{RAY} \simeq 0.25\%$. Consequently the major experimental uncertainty in the ratio

$$\left(\frac{1+\alpha}{1+\rho\alpha}\right)_{RAM} \Big/ \left(\frac{1+\alpha}{1+\rho\alpha}\right)_{RAY}$$

is contributed by the uncertainty in the spectrometer polarization response α. Observed fluctuation in this measurement within 2%, which is consistent with the S.D. of count totals involved in the determination of α. The consequent error in the ratio is about 1%. Combining these error contributions in accordance with Eq.(C-5), we obtain

$$\frac{\Delta(F\sigma)x}{(F\sigma)x} \simeq 8\%$$

Error Estimates for O_2 and CO_2 Cross Section Measurements

Measurements of the O_2 RRS cross sections and U-values relative to N_2 are expected to be the most accurate values reported here, because these measurements require less than one hour (after preliminary alignment) and involve simply a ratio of count rates. The only significant error should be that contributed by the S.D. of count rates, which yields a measurement S.D. of 5% for $U(O_2,\lambda_o)/U(N_2,\lambda_o)$.

Expected errors in the CO_2 measurements are larger because of the necessity to de-convolve the slit function from the observed signal in order to obtain the contribution of a single line. Past experience with this procedure leads us to expect an error of about 10% in the result for $U(CO_2,\lambda_o)/U(N_2,\lambda_o)$.

The absolute values $U(O_2,\lambda_o)$ and $U(CO_2,\lambda_o)$ are obtained in principle by multiplying the ratios discussed above by $U(N_2,\lambda_o)$ and thus their expected errors depend on that of this quantity, as well as that of the ratios. Combining these error contributions in accordance with Eq.(C-5) we obtain

$$\frac{\Delta U(O_2,\lambda_o)}{U(O_2,\lambda_o)} \simeq 10\%$$

and

$$\frac{\Delta U(CO_2, \lambda_o)}{U(CO_2, \lambda_o)} \simeq 12\ \%$$

Error Estimates for Depolarization Measurements

Depolarization is calculated from Eq. 61, which involves α and the counts C^s and C^s. Consequently

$$\frac{\Delta\rho}{\rho} \simeq \left[\left(\frac{d\rho}{dC^s}\ \Delta C^s\right)^2 + \left(\frac{d\rho}{dC^s}\ \Delta C^s\right)^2 + \left(\frac{d\rho}{d\alpha}\ \Delta\alpha\right)^2\right]^{1/2}$$

The error estimates for depolarization measurements in Table 7 are calculated from this expression, with the assumption that $\frac{\Delta\alpha}{\alpha} = 2\%$.

APPENDIX D. SYMBOLS

In this appendix symbols introduced in the main text of this report are presented in alphabetical order.

Symbol	Definition	Equation where first used
B_o	Rotational constant in cm^{-1}, determining energy separation of rotational states	9
B_λ	Surface brightness viewed along the normal to the surface (watts/cm^2 sr nm)	35
$b_{J\to J'}$	Placzek-Teller coefficient for the transition $J\to J'$	16
$b(J,N;J',N')$	Placzek-Teller coefficient including electronic angular momentum	
C_o	Signal count rate in response to reference light with no polarization analyzer	36
$C_\perp$	Signal count rate in response to reference light with polarization analyzer oriented perpendicular to grating grooves	37
$C_\parallel$	Signal count rate in response to reference light with polarization analyzer oriented parallel to grating grooves	38
C_o^s	Signal count rate in response to scattered light without polarization analyzer	41
$C_\perp^s$	Signal count rate in response to scattered light with polarization analyzer oriented in z-direction of Fig. 1 (which is perpendicular to grating grooves)	42
$C_\parallel^s$	Signal count rate in response to scattered light with polarization analyzer oriented in x-direction of Fig. 1 (which is parallel to grating grooves)	43
C_1	Count rate in response to scattered light with no analyzer and incident beam polarization perpendicular to direction of observation	60
C_2	Count rate in response to scattered light with no analyzer and incident beam polarization parallel to direction of observation	60

Symbol	Definition	Equation where first used
$C(\lambda)$	Relative count rate as a function of scattered light wavelength	48
c	Speed of light	15
D	Ratio of line intensities	46
$(D_z)_{ij}$	Matrix element between states i and j for z-component of dipole moment	55
$D(\lambda)$	Ratio of integrated line intensity for CO_2 to standard line intensity for N_2 as a function of center wavelength λ of scattered light band-pass for CO_2	49
E_J	Rotational energy of molecule in a state with quantum number J	13
F	Fraction of molecules in initial states which contribute to observed scattering	1
F_J	Fraction of molecules in the initial states which contribute to an observed rotational Raman line	12
G		64
g_J	Statistical weight of the rotational level with quantum number J	13
h	Planck constant	15
$I_{J\to J'}$	Intensity of rotational Raman line associated with the transition from rotational level J to rotational level J'	
I_j^R	Intensity of scattered light with polarization in j-direction (j=x,z) and polarization of incident beam in rotated state (i.e. parallel to direction of observation)	
I_s	Intensity of scattered light (e.g. watts/steradian)	1
I_x	Intensity of light scattered in the y-direction with polarization in the x-direction (See Fig. 1)	3
I_z	Intensity of light scattered in y-direction with polarization in z-direction (See Fig. 1)	3

Symbol	Definition	Equation where first used
$(I_z)_{J\to J'}$	Intensity of rotation Raman scattering with polarization in z-direction (direction of polarization of incident light) associated with a transition from J to J'	20
I_λ	Spectral irradiance of calibration lamp at diffusing surface (watts/cm^2 nm)	35
J	Quantum number for total angular momentum of a molecule (neglecting nuclear spin). For nitrogen in its ground electron state, this symbol is conventionally used also for the rotational quantum number, since there are no other contributions to the angular momentum	9
k	Boltzmann's constant	13
L	Length of scattering volume, measured along incident beam	1
ℓ	Length (or height) of spectrometer entrance slit	36
M	Linear magnification of image of incident beam at the spectrometer entrance slit by collector lens	41
N	Number density of molecules in a gas sample	1
N	Rotational angular momentum quantum number for oxygen	46
n	Refractive index of gas	34
P_o	Power of incident light beam	1
P_o	Power of incident beam, measured after incident beam passes through cell	
p	Gas pressure	46
Q	Rotational partition function	13
$R_{\parallel}$	Spectrometer system response to light with polarization parallel to grating grooves	36
$R_{\perp}$	Spectrometer system response to light with polarization perpendicular to grating grooves	36

Symbol	Definition	Equation where first used
S		27
S_Q		26
SAS		25
S_S		24
$(S.D.)_{J\to J'}$	Theoretical standard deviations for RRS line intensities	67
T_p	Transmission of polarizer to aligned polarized light	38
$T^R_{J\to J'}$	Theoretical count rate	66
$T^{UR}_{J\to J'}$	Theoretical count rate	
T_1	Transmission of scattering cell window closest to spectrometer	36
T_2	Transmission of scattering cell window opposite spectrometer	36
T_4	Transmission of scattering cell wall where incident beam exits	41
U	A factor which expresses that part of the rotational Raman cross section which is nearly independent of incident wavelength and rotational quantum number	16
$U(Z,\lambda_o)$	U-value for gas Z measured at incident wavelength λo	47
w	Spectrometer entrance slit width	36
w_e	Spectrometer exit slit width	36
X	Ratio of calculated Rayleigh scattering cross section (from refractive index) to (absolute) measured value	
Z	Ratio of RRS line to Rayleigh line	
α	Parameter expressing polarization response of spectrometer	39

Symbol	Definition	Equation where first used
Δ	Reciprocal dispersion of spectrometer (in nm/mm)	36
$\dot{\Theta}$	Absolute temperature	13
λ_o	Wavelength of incident light	34
μ	Angle between spectrometer axis and direction along which any particular ray of reference light passes through the scattering cell	36
ρ	Depolarization of light scattered from a linearly polarized incident beam into a direction perpendicular to directions of polarization and propagation of the incident beam	2
ρ_q	Theoretical depolarization of quadrupole scattering	23
ρ_{RAY}	Depolarization of Rayleigh scattering	32
ρ_T	Depolarization of composit of Rayleigh and rotational Raman scattering	33
ρ'	Depolarization of light scattered from an unpolarized incident beam into a direction perpendicular to the direction of propagation of the incident beam	5
σ	Differential cross section (cross section per unit solid angle) for light scattering. Typical units cm^2/steradian	1
σ^T	Cross section for light scattering integrated over all angles	8
σ^t	Differential cross section (cm^2/sr) for trace scattering	29
σ_{zz}	Differential cross section for light scattered with same polarization direction as incident beam	2
$(\sigma_{zz})_{RAY}$	Cross section for Rayleigh scattering	34
Ψ	Angle between polarization directions of incident and scattered light	2

Symbol	Definition	Equation where first used
Ω	Average solid angle of light accepted by spectrometer	36
$\omega_{J \to J'}$	Energy difference (in cm^{-1}) between J and J' rotational states	9
ω_{ij}	Energy difference (in cm^{-1}) between quantum states i and j	55
ω_o	Wave number of incident light (in cm^{-1})	16

REFERENCES

1. Cooney, John: Measurement of Atmospheric Temperature Profiles by Raman Backscatter. J. Appl. Meteor., vol. 9, Feb. 1972, pp. 108-112.

2. Salzman, Jack A.; Masica, William J,; and Coney, Thom A.: Determination of Gas Temperatures from Laser-Raman Scattering. NASA TN D-6336, 1971.

3. Maier, M.; Kaiser, W.; Giordmaine, J.A.: Backward Stimulated Raman Scattering. Phys. Rev., vol. 177, no. 2, Jan. 1969, pp. 580-599.

4. Ory, Horace A.; and Yura, Harold T.: Rayleigh and Raman Scattering in Molecular Nitrogen. RM-4664-ARPA, The Rand Corp., Aug. 1965.

5. Weber, Alfons; Porto, Sergio P.S.; Cheesman, Leonard E.; and Barrett, Joseph J.: High-Resolution Raman Spectroscopy of Gases with cw-Laser Excitation. J. Opt. Soc. Am., vol. 57, no. 1, Jan. 1967, pp. 19-28.

6. Rudder, Ralph R.; and Bach, David R.: Rayleigh Scattering of Ruby-Laser Light by Neutral Gases. J. Opt. Soc. Am., vol. 58, no. 9, Sep. 1968, pp. 1260-1266.

7. Ishiguro, Eiichi; Arai, Tadashi; Mizuchima, Masataka; and Kotani, Masao: On the Polarizability of the Hydrogen Molecule. Proc. Phys. Soc. (London), vol. 65A, 1952, pp. 178-187.

8. Penney, Carl M.: Light Scattering in Terms of Oscillator Strengths and Refractive Indices. J. Opt. Soc. Am., vol. 59, no. 1, 1969, pp. 34-42.

9. Placzek, G.: The Rayleigh and Raman Scattering. UCRL Trans No. 526 (L), Lawrence Radiation Laboratory, 1959. (English translation from Handbuch der Radiologie, vol. VI, 2, 1934, pp. 209-374.).

10. Herzberg, Gerhard: Molecular Spectra and Molecular Structure. Vol. I. Spectra of Diatomic Molecules, Second Edition, D. Van Nostrand Co., Inc., 1950.

11. Renschler, D.L.; Hunt, J.L.; McCubbin, Jr., T.K.; and Polo, S.R.: Triplet Structure of the Rotational Raman Spectrum of Oxygen. J. Mol. Spectry, vol. 31, no. 1, July 1969, pp. 173-176.